

Integrability vs non-integrability

Hard hexagons and hard squares compared

M. Assis¹, J.L. Jacobsen^{2,3}, I. Jensen⁴, J-M. Maillard⁵ and B.M. McCoy¹

¹ CN Yang Institute for Theoretical Physics, State University of New York, Stony Brook, NY, 11794, USA

² Laboratoire de Physique Théorique, École Normale Supérieure, 24 rue Lhomond, 75231 Paris Cedex, France

³ Université Pierre et Marie Curie, 4 Place Jussieu, 75252 Paris, France

⁴ ARC Center of Excellence for Mathematics and Statistics of Complex Systems, Department of Mathematics and Statistics, The University of Melbourne, VIC 3010, Australia

⁵ LPTMC, UMR 7600 CNRS, Université de Paris, Tour 23, 5ème étage, case 121, 4 Place Jussieu, 75252 Paris Cedex 05, France

Abstract.

In this paper we compare the integrable hard hexagon model with the non-integrable hard squares model by means of partition function roots and transfer matrix eigenvalues. We consider partition functions for toroidal, cylindrical, and free-free boundary conditions up to sizes 40×40 and transfer matrices up to 30 sites. For all boundary conditions the hard squares roots are seen to lie in a bounded area of the complex fugacity plane along with the universal hard core line segment on the negative real fugacity axis. The density of roots on this line segment matches the derivative of the phase difference between the eigenvalues of largest (and equal) moduli and exhibits much greater structure than the corresponding density of hard hexagons. We also study the special point $z = -1$ of hard squares where all eigenvalues have unit modulus, and we give several conjectures for the value at $z = -1$ of the partition functions.

AMS Classification scheme numbers: 34M55, 47E05, 81Qxx, 32G34, 34Lxx, 34Mxx, 14Kxx

Key-words: Hard square model, hard hexagon model, partition function zeros, equimodular curves

1. Introduction

There is a fundamental paradox in the practice of theoretical physics. We do exact computations on integrable systems which have very special properties and then apply the intuition gained to generic systems which have none of the special properties which allowed the exact computations to be carried out. The ability to do exact computations relies on the existence of sufficient symmetries which allow the system to be solved by algebraic methods. Generic systems do not possess such an algebra and the distinction between integrable and non-integrable may be thought of as the distinction of algebra versus analysis.

This paradox is vividly illustrated by the two dimensional Ising model. In zero magnetic field Onsager [1] computed the free energy by means of exploiting the algebra which now bears his name. On the other hand in 1999 Nickel [2, 3] analyzed the expansion of the susceptibility at zero magnetic field for the isotropic Ising model on

the square lattice and discovered that as a function of the variable $s = \sinh 2E/k_B T$ the susceptibility has a dense set of singularities on the circle $|s| = 1$ which is the same location as the thermodynamic limit of the locus of zeros of the finite lattice partition function. From this Nickel concluded that the curve of zeros is a natural boundary of the susceptibility in the complex s plane. This is a phenomenon of analysis not seen in any previously solved statistical system. Further study of this new phenomenon has been made by Orrick, Nickel, Guttman and Perk [4] and in [5] the phenomenon of the natural boundary was studied on the triangular lattice. However the implication of these results for other models has not been investigated.

The hard square and hard hexagon models can be obtained from the Ising model in a magnetic field H in the limit $H \rightarrow \infty$ for the square and triangular lattices respectively, and thus it is natural to study the question of analyticity in these two models. However, unlike the Ising model at $H = 0$ where both the square and triangular lattices have been exactly solved, the hard hexagon model is exactly solved [6]-[8] whereas the hard square model is not. Thus, the comparison of these two models is the ideal place to study the relation of integrability to the analyticity properties of the free energy in the complex plane.

Three different methods may be used to study the non-integrable hard square model: Series expansions of the free energy in the thermodynamic limit, transfer matrix eigenvalues for chains of finite size L_h and zeros of partition functions on the $L_v \times L_h$ lattices of finite size and arbitrary aspect ratio L_v/L_h .

Series expansions of the partition function per site $\kappa(z)$ of the hard square model [9]-[14] of up to 92 terms [13] and analysis of transfer matrix eigenvalues [12] for chains of up to 34 sites [15] show that $\kappa(z)$ has a singularity on the positive z -axis [15]

$$z_c = 3.79625517391234(4) \quad (1)$$

and a singularity on the negative z -axis [16, 17]

$$z_d = -0.119338886(5) \quad (2)$$

The hard hexagon model has two singular points at [6]-[8]

$$\begin{aligned} z_{c;hh} &= \frac{11 + 5\sqrt{5}}{2} = 11.09016\dots \\ z_{d;hh} &= \frac{11 - 5\sqrt{5}}{2} = -0.09016\dots \end{aligned} \quad (3)$$

For hard squares, series expansions [9]-[14] have been used to estimate the leading critical exponents at z_c and z_d , and correction to scaling exponents have been estimated as well. For hard hexagons there are no singular points of the free energy other than $z_{c;hh}$, $z_{d;hh}$, ∞ . It is not known if there are any further singular points for hard squares. In [15] the singularity at z_c is determined to be in the Ising universality class and in [17] the first two exponents at z_d are shown to agree with those of the Lee-Yang edge and hard hexagons. However these long series expansions have not given information about additional higher order singularities at z_c and z_d or singularities which may occur at other values of z .

In 2005 a very remarkable property of hard squares, which is not shared by hard hexagons, was discovered [18] by means of studying the eigenvalues of the transfer matrix for finite size systems [18]-[23]. These studies discovered that at the value of the fugacity $z = -1$ all eigenvalues of the transfer matrix with cylindrical boundary conditions have unit modulus and the partition function of the $L_h \times L_v$

lattice with toroidal boundary conditions depends on divisibility properties of L_v and L_h . However, the free energy for these boundary conditions in the thermodynamic limit is zero. For the lattice oriented at 45° , on the other hand, for cylindrical boundary conditions of the transfer matrix, there are some eigenvalues which do not have unit modulus [20] and for free boundary conditions of the transfer matrix with $L_h \equiv 1 \pmod{3}$ all roots of the characteristic equation are zero and thus the partition function vanishes.

In [24] we computed for hard hexagons the zeros of the partition function for $L \times L$ lattices with cylindrical and toroidal boundary conditions as large as 39×39 and the eigenvalues of the transfer matrix with cylindrical boundary conditions. For these cylindrical transfer matrices both momentum and parity are conserved, and for physical (positive) values of z the maximum eigenvector is in the sector of zero momentum positive parity $P = 0^+$. From these cylindrical transfer matrices we computed the equimodular curves where there are two eigenvalues of the row transfer matrix of (equal) maximum modulus both in the sector $P = 0^+$ and for the full transfer matrix.

In this paper we extend our study of partition function zeros and transfer matrix equimodular curves to hard squares for systems as large as 40×40 and compare them with corresponding results for hard hexagons [24]. There are many differences between these two systems which we analyze in detail. In addition to the transfer matrix with cylindrical boundary conditions we also introduce the transfer matrix with free boundary conditions. Thus we are able to give two different transfer matrix descriptions for the partition function zeros of the cylindrical lattice. For hard hexagons there is strong evidence that this boundary condition preserves integrability.

In section 2 we recall the relation between finite size computations in the complex plane of zeros of $L \times L$ lattices and eigenvalues of the L site transfer matrix. In section 3 we make a global comparison in the complex z plane of the equimodular curves and partition function zeros of hard squares with hard hexagons. In section 4 we make a more refined comparison on the negative z axis.

The comparisons presented in sections 3 and 4 reveal many significant differences between hard squares and hard hexagons which we discuss in detail in section 5. We conclude in section 6 with a presentation of potential analyticity properties of hard squares which can be different from hard hexagons.

In Appendix A we tabulate the factored characteristic polynomials of the transfer matrix at the point $z = -1$ and the multiplicity of the eigenvalue $+1$. We also give formulas for the growth of the orders of the transfer matrices, where such a formula is known, and for all cases the asymptotic growth is given by $N_G^{L_h}$ where N_G is the golden ratio.

In Appendix B we consider the partition function values at $z = -1$ on $L_v \times L_h$ lattices for the torus, cylinder, free-free rectangle, Möbius band and Klein bottle boundary conditions. We give generating functions for the sequences of values of the partition function of the $L_v \times L_h$ lattice as a function of L_v and find that almost all sequences of values are repeating. We conjecture that along the periodic L_v direction (including twists for the Möbius band and Klein bottle cases) the sequences will always be repeating. Furthermore, for the torus and the cylinder (along the periodic L_v direction), we conjecture that the generating functions are given by the negative of the logarithmic derivative of the characteristic polynomial of their transfer matrices at $z = -1$. This allows us to conjecture the periods of their repeating sequences. Finally, for the Möbius band (along the periodic L_v direction) and Klein bottle we conjecture

that their generating functions are the logarithmic derivative of products of factors $(1 - x^{n_i})^{m_j}$, where n_i , m_j are integers.

2. Formulation

The hard square lattice gas is defined by a (occupation) variable $\sigma = 0, 1$ at each site of a square lattice with the restriction that no two adjacent sites can have the values $\sigma = 1$ (i.e. the gas has nearest neighbor exclusion). The grand partition function on the finite $L_v \times L_h$ lattice is defined as the polynomial

$$Z_{L_v, L_h}(z) = \sum_{n=0} z^n g(n; L_v, L_h). \quad (4)$$

where $g(n; L_v, L_h)$ is the number of hard square configurations which have n occupied sites. These polynomials can be characterized by their zeros z_j as

$$Z_{L_v, L_h}(z) = \prod_j (1 - z/z_j), \quad (5)$$

where z_j and the degree of the polynomial will depend on the boundary condition imposed on the lattice. This formulation of the partition function as a polynomial is completely general for lattice models with arbitrary interactions.

The partition function for hard squares may also be expressed in terms of the transfer matrix formalism. For the cylindrical transfer matrix with periodic boundary conditions in the horizontal direction, the transfer matrix for hard squares is defined as

$$T_{C\{b_1, \dots, b_{L_h}\}, \{a_1, \dots, a_{L_h}\}}(z; L_h) = \prod_{j=1}^{L_h} W(a_j, a_{j+1}; b_j, b_{j+1}), \quad (6)$$

where the local Boltzmann weights $W(a_j, a_{j+1}; b_j, b_{j+1})$ for hard squares of figure 1 may be written as

$$W(a_j, a_{j+1}; b_j, b_{j+1}) = 0 \text{ for } a_j a_{j+1} = a_{j+1} b_{j+1} = b_j b_{j+1} = a_j b_j = 1 \quad (7)$$

with $a_{L_h+1} \equiv a_1$, $b_{L_h+1} \equiv b_1$ and otherwise

$$W(a_j, a_{j+1}; b_j, b_{j+1}) = z^{b_j}. \quad (8)$$

For the transfer matrix with free boundary conditions

$$T_{F\{b_1, \dots, b_{L_h}\}, \{a_1, \dots, a_{L_h}\}}(z; L_h) = \left(\prod_{j=1}^{L_h-2} W(a_j, a_{j+1}; b_j, b_{j+1}) \right) W_F(a_{L_h-1}, a_{L_h}; b_{L_h-1}, b_{L_h}), \quad (9)$$

where

$$W_F(a_{L_h-1}, a_{L_h}; b_{L_h-1}, b_{L_h}) = z^{b_{L_h-1} + b_{L_h}}. \quad (10)$$

The corresponding transfer matrices for hard hexagons are obtained by supplementing (7) with

$$W(a_j, a_{j+1}; b_j, b_{j+1}) = 0 \text{ for } a_{j+1} b_j = 1. \quad (11)$$

We will consider four types of boundary conditions.

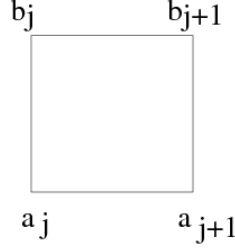


Figure 1. Boltzmann weights for the transfer matrix of hard squares

The grand partition function for $L_v \times L_h$ lattices with periodic boundary conditions in both the L_v and L_h directions is given in terms of T_C as

$$Z_{L_v, L_h}^{CC}(z) = \text{Tr } T_C^{L_v}(z; L_h). \quad (12)$$

For free boundary conditions in the horizontal direction and periodic boundary conditions the vertical direction the partition function is obtained from T_F as

$$Z_{L_v, L_h}^{CF}(z) = \text{Tr } T_F^{L_v}(z; L_h). \quad (13)$$

For periodic boundary conditions in the horizontal direction and free boundary conditions the vertical direction the partition function is obtained from T_C as

$$Z_{L_v, L_h}^{FC}(z) = \langle \mathbf{v}_B | T_C^{L_v-1}(z; L_h) | \mathbf{v}'_B \rangle, \quad (14)$$

where \mathbf{v}_B and \mathbf{v}'_B are suitable vectors for the boundary conditions on rows 1 and L_v . For the transfer matrix (6) with Boltzmann weights given by the asymmetrical form (7), (8) the components of the vectors \mathbf{v}_B and \mathbf{v}'_B for free boundary conditions are

$$\mathbf{v}_B(a_1, a_2, \dots, a_{L_h}) = \prod_{j=1}^{L_h} z^{a_j}, \quad \mathbf{v}'_B(b_1, b_2, \dots, b_{L_h}) = 1. \quad (15)$$

These vectors are invariant under translation and reflection.

For free boundary conditions in both directions

$$Z_{L_v, L_h}^{FF}(z) = \langle \mathbf{v}_B | T_F^{L_v-1}(z; L_h) | \mathbf{v}'_B \rangle, \quad (16)$$

When the transfer matrix is diagonalizable (12)-(16) may be written in terms of the eigenvalues λ_k and eigenvectors \mathbf{v}_k of the transfer matrix

$$Z_{L_v, L_h}^{CC}(z) = \sum_k \lambda_{k;C}^{L_v}(z; L_h), \quad (17)$$

$$Z_{L_v, L_h}^{CF}(z) = \sum_k \lambda_{k;F}^{L_v}(z; L_h), \quad (18)$$

$$Z_{L_v, L_h}^{FC}(z) = \sum_k \lambda_{k;C}^{L_v-1}(z; L_h) \cdot d_{C,k} \quad \text{where } d_{C,k} = (\mathbf{v}_B \cdot \mathbf{v}_{C,k})(\mathbf{v}_{C,k} \cdot \mathbf{v}'_B), \quad (19)$$

$$Z_{L_v, L_h}^{FF}(z) = \sum_k \lambda_{k;F}^{L_v-1}(z; L_h) \cdot d_{F,k} \quad \text{where } d_{F,k} = (\mathbf{v}_B \cdot \mathbf{v}_{F,k})(\mathbf{v}_{F,k} \cdot \mathbf{v}'_B). \quad (20)$$

For hard squares and hard hexagons the transfer matrices $T_C(z; L_h)$ are invariant under translations and reflections and thus momentum P and parity \pm are good quantum numbers. Furthermore the boundary vectors \mathbf{v}_B and \mathbf{v}'_B of (15) are invariant

under translation and reflection, and consequently $d_{C,k} = 0$ unless the eigenvectors \mathbf{v}_k lie in the positive parity sector $P = 0^+$.

For hard squares the matrix $T_F(z; L_h)$ is invariant under reflection so the eigenvectors in the scalar products are restricted to positive parity states. However for hard hexagons $T_F(z; L_h)$ is not invariant under reflection and all eigenvectors will contribute to (20).

Note that partition function zeros for all four boundary conditions have previously been studied for antiferromagnetic Potts models [25]-[29]. In that case the relations to transfer matrix eigenvalues were similar to (19),(20). However, with periodic boundary conditions along the transfer direction the partition function was defined as a Markov trace, and (17),(18) were replaced by expressions involving non-trivial eigenvalue multiplicities [30, 31].

2.1. Integrability

To compare integrable with non-integrable systems a definition of integrability is required.

The notion of integrability originates in the discovery by Baxter that the Ising model and the 6 and 8 vertex models, which have transfer matrices that depend on several variables, have a one parameter subspace for which the transfer matrices with different parameters will commute if cyclic boundary conditions are imposed [7]. This global property of the transfer matrix follows from a local property of the Boltzmann weights used to construct the transfer matrix, known as the star-triangle or the Yang-Baxter equation.

The hard hexagon model has only one parameter, the fugacity, but is also referred to as integrable because Baxter [6, 7] found that it may be realized as a special case of the model of hard squares with diagonal interactions which does have a one parameter family of commuting transfer matrices with cylindrical boundary conditions.

This concept of integrability has been generalized to transfer matrices with boundary conditions which are not cylindrical if special boundary conditions are imposed which satisfy a generalization of the Yang-Baxter equation [32, 33] known as the boundary Yang-Baxter equation. This has been investigated for models closely related to hard hexagons [34, 35] but the specialization to hard hexagons with free boundary conditions has apparently not been made.

2.2. The physical free energy

For thermodynamics we are concerned with the limit $L_v, L_h \rightarrow \infty$, and in the physical region where z is real and positive the partition function per site $\kappa(z)$, the physical free energy $F(z)$ and the density $\rho(z)$ are defined as limits of the finite size grand partition function as

$$\kappa(z) = \lim_{L_v, L_h \rightarrow \infty} Z_{L_v, L_h}(z)^{1/L_v L_h}, \quad (21)$$

$$-F(z)/k_B T = \lim_{L_v, L_h \rightarrow \infty} (L_v L_h)^{-1} \cdot \ln Z_{L_v, L_h}(z) \quad (22)$$

and

$$\rho(z) = -z \frac{d}{dz} F(z). \quad (23)$$

This limit must be independent of the boundary conditions and aspect ratio $0 < L_v/L_h < \infty$ for thermodynamics to be valid. The free energy vanishes and is analytic at $z = 0$. For hard hexagons as $z \rightarrow \infty$

$$F(z)/k_B T = \frac{1}{3} \ln z + \tilde{F}_{HH}(z) \quad \text{and} \quad \rho(z) \rightarrow \frac{1}{3} \quad (24)$$

and for hard squares

$$F(z)/k_B T = \frac{1}{2} \ln z + \tilde{F}_{HS}(z) \quad \text{and} \quad \rho \rightarrow \frac{1}{2}, \quad (25)$$

where $\tilde{F}_{HH}(z)$ and $\tilde{F}_{HS}(z)$ are analytic at $z \rightarrow \infty$. From this formulation series expansions of the free energy about both $z = 0$ and $1/z = 0$ are derived. The partition function per site, physical free energy and density for $0 \leq z \leq z_c$ and $z_c \leq z \leq \infty$ are different functions which are not related to each other by analytic continuation around the singularity at z_c . For hard hexagons the density for both the low and the high density regime may be continued to the full z plane which for low density is cut from $-\infty \leq z \leq z_{d;hh}$ and $z_{c;hh} \leq z \leq \infty$ and for high density cut from $z_{d;hh} \leq z \leq z_{c;hh}$. Indeed, both the low and high density partition functions per site and the density for hard hexagons are algebraic functions [36, 24] and thus have analytic continuations even beyond the cuts in the z plane.

To study the possibility of analytic continuation for hard squares of the physical partition function per site and density from the positive z axis into the complex z plane we consider both the formulation in terms of the transfer matrix and the zeros of the partition function.

2.3. Analyticity and transfer matrix eigenvalues

For $0 < z < \infty$ all matrix elements of the transfer matrices are positive so the Perron-Frobenius theorem guarantees that the largest eigenvalue λ_{\max} is positive and the corresponding eigenvector has all positive entries. Thus for all cases

$$\lim_{L_v \rightarrow \infty} L_v^{-1} \cdot \ln Z_{L_v, L_h}(z) = \ln \lambda_{\max}(z; L_h) \quad (26)$$

and thus the free energy is

$$-F/k_B T = \lim_{L_h \rightarrow \infty} L_h^{-1} \ln \lambda_{\max}(z; L_h). \quad (27)$$

Furthermore the cylindrical transfer matrices for both squares and hexagons have translation and reflection invariance. Therefore the eigenvalues of the lattice translation operator are e^{iP} where P , the total momentum, has the values $2\pi n/L_h$, and the eigenvalues of the reflection operator are ± 1 . Each transfer matrix eigenvalue has a definite value of P and parity and λ_{\max} has $P = 0^+$ (where $+$ indicates the reflection eigenvalue). Therefore for $0 \leq z \leq \infty$ the eigenvalue λ_{\max} of the transfer matrix T_C is the eigenvalue of an eigenvector in the sector $P = 0^+$.

To obtain the analytic continuation of the density from the positive z axis into the complex z plane we need to continue the limit as $L_h \rightarrow \infty$ of the eigenvalue with $P = 0^+$ which is maximum on the positive axis. However, the analytic continuation of λ_{\max} off of the segment $0 \leq z \leq \infty$ will not, of course, have the largest modulus in the entire complex z plane. The analytic continuation of λ_{\max} will be maximum only as long as it has the largest modulus of all the eigenvalues and ceases to be maximum when z crosses an equimodular curve where the moduli of two (or more) eigenvalues are the same. It is thus of importance to determine the thermodynamic

limit of the equimodular curves of the largest eigenvalues of the transfer matrix. In the thermodynamic limit the regions of $0 \leq z \leq z_c$ and $z_c \leq z \leq \infty$ are separated by one or more of these equimodular curves. In [24] it was seen that for hard hexagons with finite L_h the equimodular curves separate the z plane into several regions. However, because the eigenvectors with different momentum and parity lie in different subspaces only the eigenvalues corresponding to eigenvectors with $P = 0^+$ can affect the analytic continuation of the density.

For the hard square transfer matrix with free boundary conditions, $T_F(z; L_h)$, the eigenvalue λ_{\max} will lie in the positive parity sector for positive z and the analytic continuation off the positive real axis will be constrained to eigenvalues in the positive parity sector. For hard hexagons, where $T_F(z; L_h)$ is not reflection symmetric, λ_{\max} is not constrained to lie in a restricted sub-space.

It is thus clear from the formulation of the physical free energy and the density in terms of the transfer matrix that the process of analytic continuation off of the positive z axis and the taking of the thermodynamic limit do not commute. In the thermodynamic limit it is not even obvious that for a non-integrable model an analytic continuation through the limiting position of the equimodular curves is possible.

2.4. Analyticity and partition function zeros

The considerations of analytic continuation in terms of partition function zeros is slightly different because by definition polynomials are single valued. However, once the thermodynamic limit is taken the limiting locations of the zeros will in general divide the complex z plane into disconnected zero free regions. For hard squares and hard hexagons the physical segments $0 \leq z < z_c$ and $z_c < z < \infty$ lie in two separate zero free regions. The density is uniquely continuable into the zero free region and in these regions the free energy will be independent of boundary conditions and aspect ratio. For hard hexagons the density for both the low and high density cases are further continuable beyond the zero free region into the respective cut planes of section 2.2. However, for hard squares there is no guarantee that further continuation outside the zero free regions is possible.

2.5. Relation of zeros to equimodular curves

For finite lattices the partition function zeros can be obtained for $Z_{L_v, L_h}^{CC}(z)$ and $Z_{L_v, L_h}^{CF}(z)$ from (17) and (18) if all eigenvalues are known. For $Z_{L_v, L_h}^{FC}(z)$ and $Z_{L_v, L_h}^{FF}(z)$ both the eigenvalues and eigenvectors are needed to obtain the zeros from (19) and (20).

The limiting case where

$$L_v \rightarrow \infty \quad \text{with fixed} \quad L_h, \quad (28)$$

is presented in [25]-[29],[37]-[39] with various boundary conditions extending the work of [40]-[42]. In this limit (28) the partition function will have zeros when two or more maximum eigenvalues of $T(z; L_h)$ have equal moduli

$$|\lambda_1(z; L_h)| = |\lambda_2(z; L_h)|. \quad (29)$$

Consider first $Z_{L_v, L_h}^{CC}(z)$ and $Z_{L_v, L_h}^{CF}(z)$ where we see from (17) and (18) that only eigenvalues are needed. Thus, for these two cases, when only two largest eigenvalues

$\lambda_{1,2}$ need to be considered we may write

$$Z_{L_v, L_h}(z) = \lambda_1^{L_v} \left[1 + \left(\frac{\lambda_2}{\lambda_1} \right)^{L_v} + \dots \right]. \quad (30)$$

Then at values of z where $|\lambda_1| = |\lambda_2|$ with $\lambda_2/\lambda_1 = e^{i\theta}$ we have for large L_v

$$Z_{L_v, L_h}(z) = \lambda_1^{L_v} [1 + e^{i\theta L_v} + \dots] \quad (31)$$

and hence $Z_{L_v, L_h}(z)$ will have a zero close to this z when

$$e^{i\theta L_v} = -1, \quad (32)$$

that is when

$$\theta L_v = (2n + 1)\pi \quad (33)$$

with n an integer. This relation becomes exact in the limit $L_v \rightarrow \infty$. Calling z_i and z_{i+1} the values of z at two neighboring zeros on the equimodular curve we thus obtain from (33)

$$\theta(z_{i+1}) - \theta(z_i) = 2\pi/L_v. \quad (34)$$

Let $s(z)$ be the arclength along an equimodular curve. Then the derivative of $\theta(s(z))$ with respect to s is defined as the limit of

$$\frac{\Delta\theta}{\Delta s} \equiv \frac{\theta(s(z_{i+1})) - \theta(s(z_i))}{s(z_{i+1}) - s(z_i)}, \quad (35)$$

Thus, defining the density of roots on the equimodular curve as

$$D(s) = \lim_{L_v \rightarrow \infty} \frac{1}{L_v [s(z_{i+1}) - s(z_i)]}, \quad (36)$$

we find from (34) and (35) that for $L_v \rightarrow \infty$ with L_h fixed that the density of zeros on an equimodular curve is

$$\frac{d\theta(s)}{ds} = 2\pi D(s). \quad (37)$$

For $Z_{L_v, L_h}^{FC}(z)$ and $Z_{L_v, L_h}^{FF}(z)$ from (19) and (20) we have instead of (30)

$$Z_{L_v, L_h}(z) = \lambda_1^{L_v} d_1 \left[1 + \left(\frac{\lambda_2}{\lambda_1} \right)^{L_v} \frac{d_2}{d_1} + \dots \right], \quad (38)$$

with

$$\frac{d_2}{d_1} = r e^{i\psi}, \quad (39)$$

where in general $r \neq 1$. Thus writing

$$\frac{\lambda_2}{\lambda_1} = \epsilon e^{i\theta}, \quad (40)$$

the condition for a zero in the limit $L_v \rightarrow \infty$ which generalizes (32) is

$$\epsilon^{L_v} e^{i\theta L_v} r e^{i\psi} = -1, \quad (41)$$

from which we obtain

$$\epsilon = r^{-1/L_v} = e^{-\ln r/L_v} \sim 1 - \frac{\ln r}{L_v}, \quad (42)$$

$$\theta L_v + \psi = (2n + 1)\pi. \quad (43)$$

Thus as $L_v \rightarrow \infty$ the locus of zeros approaches the equimodular curve as $\ln r/L_v$ and the limiting density is still given by (37).

These considerations, however, are in general not sufficient for the study of the thermodynamic limit where instead of (28) we are interested in the limit

$$L_v \rightarrow \infty, \quad L_h \rightarrow \infty, \quad \text{with fixed } L_v/L_h \quad (44)$$

and the physical free energy must be independent of the aspect ratio L_v/L_h .

To study the limit (44) there are several properties of the dependence of the equimodular curves on L_h which need to be considered:

- (i) The derivative of the phase $\theta(s)$ on a curve can vanish as $L_h \rightarrow \infty$ on some portions of the curve;
- (ii) The number of equimodular curves can diverge as $L_h \rightarrow \infty$ and there can be regions in the z plane where they become dense;
- (iii) The length of an equimodular curve can vanish as $L_h \rightarrow \infty$.

The first of these properties is illustrated for hard hexagons in [24]. The second and third properties have been observed for antiferromagnetic Potts models in [43].

We will see that all three phenomena are present for hard squares. The roots of the $L \times L$ partition function in the limit $L \rightarrow \infty$ converge to lie on the $L_h \rightarrow \infty$ limit of the equimodular curves.

3. Global comparisons of squares and hexagons

In [24] we computed for hard hexagons the zeros for $L \times L$ lattices of $Z_{L,L}^{CC}(z)$ for toroidal boundary conditions, and for cylindrical boundary conditions where

$$Z_{L,L}^{FC}(z) = Z_{L,L}^{CF}(z). \quad (45)$$

We also computed the equimodular curves for both the full transfer matrix $T_C(z; L_h)$ relevant to $Z_{L_v, L_h}^{CC}(z)$ and the restriction to the subspace $P = 0^+$ relevant for $Z_{L_v, L_h}^{FC}(z)$. In this paper we compute the same quantities for hard squares and compare them with the results of [24]. We also compute the equimodular curves for $T_F(z; L_h)$ relevant for $Z_{L_v, L_h}^{CF}(z)$ and $Z_{L_v, L_h}^{FF}(z)$. For hard hexagons we restricted attention to L_v, L_h multiples of three which is commensurate with hexagonal ordering. Similarly for hard squares we restrict attention here to L_v, L_h even to be commensurate with square ordering.

3.1. Comparisons of partition function zeros

We have computed zeros of the hard square partition function in the complex fugacity z plane for $L \times L$ lattices with cylindrical and free boundary conditions for $L \leq 40$ and for toroidal boundary conditions for $L \leq 26$ using the methods of [24]. In figure 2 we compare partition function zeros for cylindrical boundary conditions of hard squares on the 40×40 lattice with hard hexagons on the 39×39 lattice and in figure 4 the comparison is made for free boundary conditions. In figure 3 we compare for toroidal boundary conditions hard squares on the 26×26 lattice with hard hexagons on the 27×27 lattice.

For both hard squares and hard hexagons there is a line of zeros on the negative real axis ending at z_d and $z_{d,hh}$, respectively. The ratio of real roots to complex

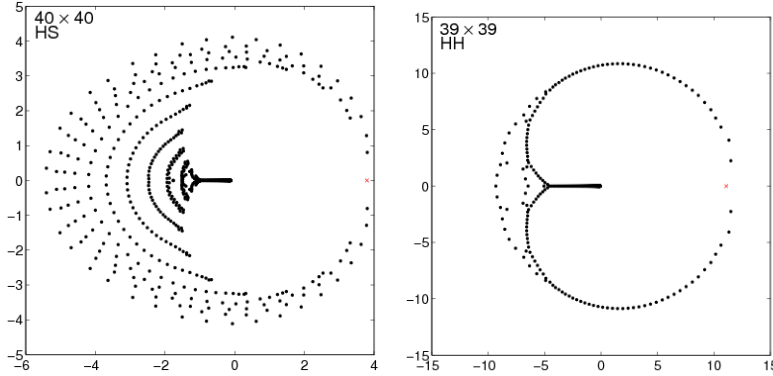


Figure 2. Comparison in the complex fugacity plane z of the zeros of the partition function $Z_{L,L}^{FC}(z) = Z_{L,L}^{CF}(z)$ with cylindrical boundary conditions of hard squares on the 40×40 lattice on the left to hard hexagons on the 39×39 lattice on the right. The location of z_c and $z_{c,hh}$ is indicated by a cross.

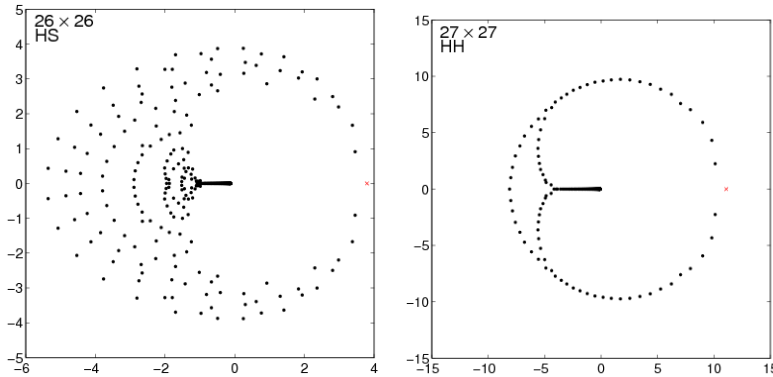


Figure 3. Comparison in the complex fugacity plane z of the zeros of the partition function $Z_{L,L}^{CC}(z)$ with toroidal boundary conditions of hard squares on the 26×26 lattice on the left to hard hexagons on the 27×27 lattice on the right. The location of z_c and $z_{c,hh}$ is indicated by a cross.

roots for hard squares is roughly $1/2:1/2$ while for hard hexagons the ratio is roughly $2/3:1/3$.

The most obvious difference between hard squares and hard hexagons in figures 2-4 is that the zeros of hard squares are seen to lie in an area instead of being confined to a few well defined curves as is seen for hard hexagons.

For cylindrical boundary conditions the filling up of this area proceeds in a remarkably regular fashion.

For the lattices $4N \times 4N$ there are $N - 1$ outer arcs each of $4N$ points, then there is a narrow arclike area with close to $4N$ zeros and finally there is an inner structure that is connected to $z = -1$. For the innermost of the $N - 1$ arcs the zeros appear in well defined pairs.

For lattices $(4N + 2) \times (4N + 2)$ there are $N - 1$ outer arcs each of $4N + 2$ points, then a narrow arclike area which has close to $4N + 2$ zeros and finally an inner

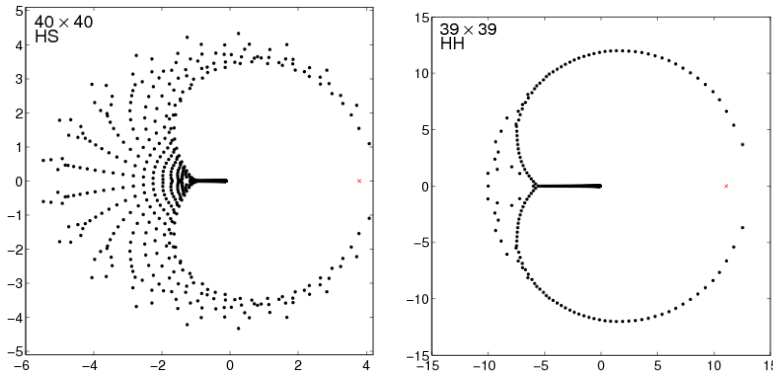


Figure 4. Comparison in the complex fugacity plane z of the zeros of the partition function $Z_{L,L}^{FF}(z)$ with free boundary conditions of hard squares on the 40×40 lattice on the left to hard hexagons on the 39×39 lattice on the right. The location of z_c and $z_{c;hh}$ is indicated by a cross.

structure that is connected to $z = -1$.

For all boundary conditions the zeros of hard squares appear to converge in the $L \rightarrow \infty$ limit to a wedge which hits the positive z axis at z_c . This is distinctly different from the behavior of hard hexagons where the zeros appear to approach $z_{c;hh}$ on a well defined one dimensional arc.

In figure 5 we illustrate the dependence on L of the hard square zeros of $Z_{L,L}^{FC}(z) = Z_{L,L}^{CF}(z)$ of the $L \times L$ lattice by giving a combined plot of all the zeros for $12 \leq L \leq 40$. This reveals that the three cases of $L = 6n + 4$, $6n + 2$ and $6n$ approach the common limit in three separate ways. There is one well defined curve whose position does not depend on L which consists only of the points of $L = 6n + 4$ lattices.

In table 1 we list the value of the zero closest to the three endpoints z_c , z_d and -1 for the $L \times L$ cylindrical lattices with $24 \leq L \leq 40$. We also list the number N_L of zeroes in $-1 \leq z \leq z_d$ plus the number of zeroes $z < -1$. For $L = 40$ we note that $\text{Re}[z_c(40)] > z_c$ whereas for $L \leq 38$ we have $\text{Re}[z_c(L)] < z_c$. This behavior of $z_c(L)$ in relation to z_c is similar to what is seen for hard hexagons in table 5 of [24] where $\text{Re}[z_c(L)] > z_c$ for $L \geq 21$ and only starts to approach z_c from the right for $L = 36$.

3.2. Comparisons of equimodular curves with partition zeros

We have computed equimodular curves for the hard square transfer matrix $T_C(z; L_h)$ in the sector $P = 0^+$ for even $L_h \leq 26$ and for the full transfer matrix for $L_h \leq 18$. For hard squares we have computed the equimodular curves for the full $T_F(z; L_h)$ and the restriction to the positive parity sector for $L_h \leq 16$. For hard hexagons the equimodular curves of $T_C(z; L_h)$ were computed in [24] for $L_h \leq 21$ and in the sector $P = 0^+$ for $L_h \leq 30$. Equimodular curves for the hard hexagon transfer matrix $T_F(z; L_h)$ are computed here for $L_h \leq 21$.

In figure 6 we plot the equimodular curves and zeros for hard squares. This is to be compared with the similar plot for hard hexagons in figure 7. In both cases we note that the zeros for $Z_{L,L}^{FC}(z)$ and $Z_{L,L}^{CF}$ are identical while the corresponding equimodular curves are different.

L	$z_c(L)$	$z_d(L)$	$z_{-1}(L)$	N_L
24	$3.690334 \pm i1.324109$	-0.119976	-0.956723	$128 + 0$
26	$3.718433 \pm i1.226238$	-0.119871	-0.979835	$153 + 5$
28	$3.739986 \pm i1.141529$	-0.119788	-0.986589	$176 + 0$
30	$3.756751 \pm i1.067554$	-0.119723	-0.991656	$201 + 5$
32	$3.769947 \pm i1.002431$	-0.119671	-0.992168	$231 + 1$
34	$3.780438 \pm i0.944686$	-0.119628	-0.989045	$259 + 9$
36	$3.788852 \pm i0.893150$	-0.119592	-0.976523	$288 + 0$
38	$3.795647 \pm i0.846884$	-0.119563	-0.994325	$325 + 9$
40	$3.801169 \pm i0.805129$	-0.119538	-0.991673	$358 + 0$
∞	3.796255	-0.119338	-1	

Table 1. The endpoints $z_c(L)$, $z_d(L)$ and $z_{-1}(L)$ for the $L \times L$ cylindrical lattices with $24 \leq L \leq 40$. The number of zeros N_L on the segment $-1 \leq z \leq z_d$ as well as the very small number of points $z \leq -1$ which do not contribute to the density.

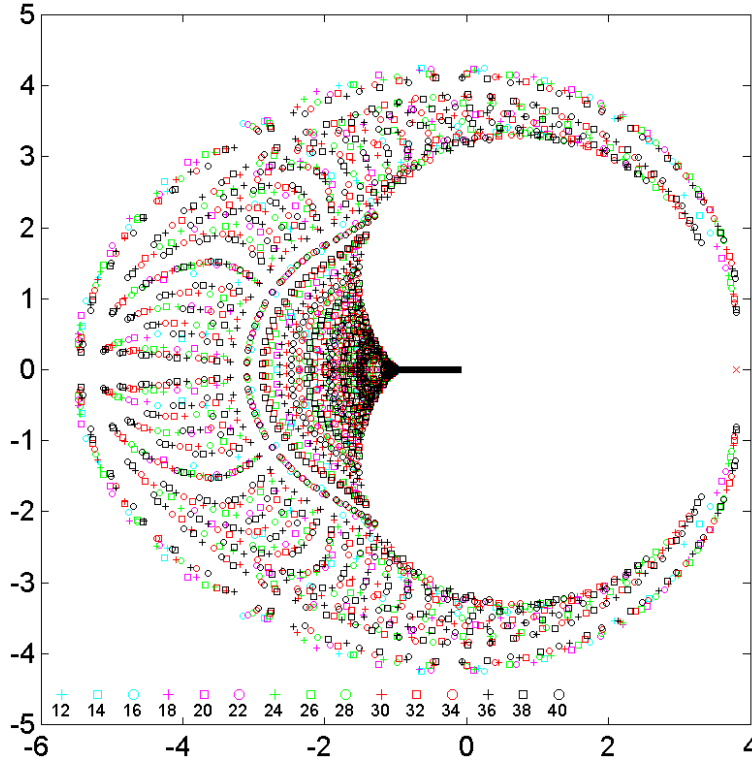


Figure 5. Combined plot of hard square zeros of $Z_{L,L}^{CF}(z) = Z_{L,L}^{FC}(z)$ for the $L \times L$ lattice with cylindrical boundary conditions for $12 \leq L \leq 40$. We exhibit a mod six effect by plotting $L = 6n + 4$ as circles, $L = 6n + 2$ as boxes and $L = 6n$ as crosses. The values of L_h are shown in the different colors indicated in the legend. It is to be noticed that there is a distinguished curve where only points $L = 6n + 4$ lie. The location of z_c is indicated by a cross.

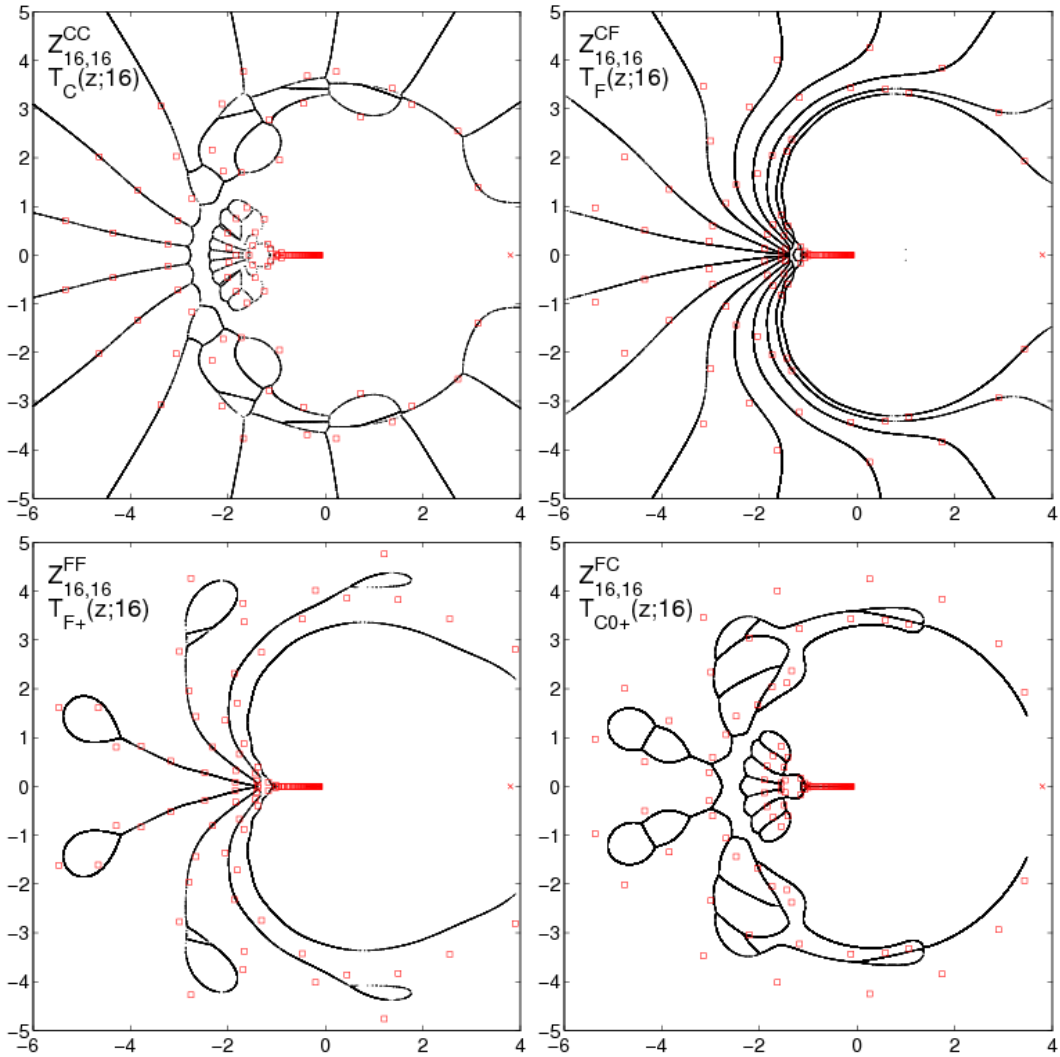


Figure 6. Comparison for hard squares of the three types of zeros and the 4 types of equimodular curves. Clockwise from the upper left we have for $L = 16$: $Z_{L,L}^{CC}(z)$ with $T_C(z;L)$, $Z_{L,L}^{CF}(z)$ with $T_F(z;L)$, $Z_{L,L}^{FC}(z)$ with $T_C(z;L)$ restricted to $P = 0^+$ and $Z_{L,L}^{FF}(z)$ with $T_F(z;L)$ restricted to positive parity. We note that the zeros of $Z_{L,L}^{FC}(z)$ and $Z_{L,L}^{CF}(z)$ are identical even though the equimodular curves are very different. The location of z_c is indicated by a cross.

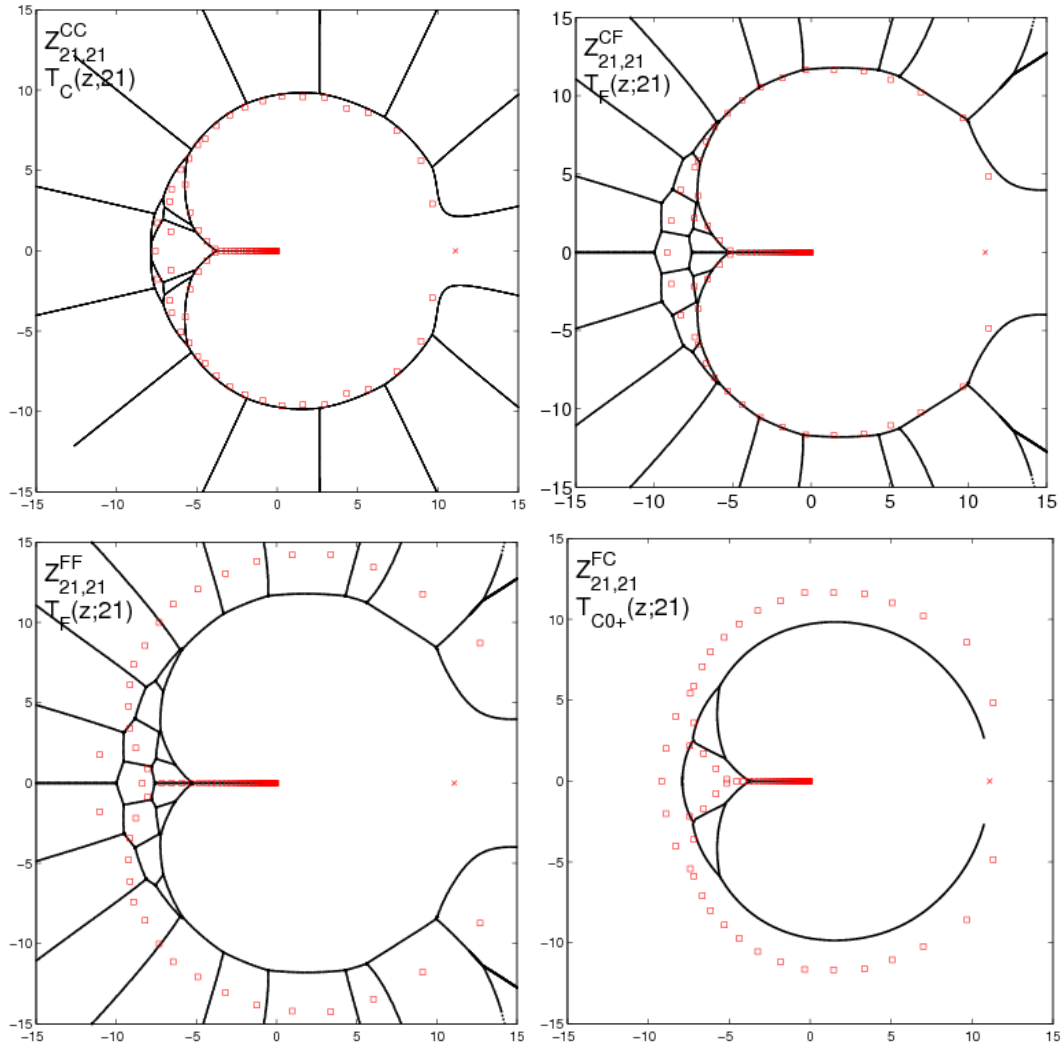


Figure 7. Comparison for hard hexagons of the three types of zeros and the 3 types of equimodular curves. Clockwise from the upper left we have for $L = 21$: $Z_{L,L}^{CC}(z)$ with $T_C(z;L)$, $Z_{L,L}^{CF}(z)$ with $T_F(z;L)$, $Z_{L,L}^{FC}(z)$ with $T_C(z;L)$ restricted to $P = 0^+$ and $Z_{L,L}^{FF}(z)$ with $T_F(z;L)$. We note that the zeros of $Z_{L,L}^{FC}(z)$ and $Z_{L,L}^{CF}(z)$ are identical even though the equimodular curves are very different. The location of $z_{c;hh}$ is indicated by a cross.

The equimodular curves of hard squares are strikingly different from those of hard hexagons for all cases considered. The hard hexagon plots consist of a few well defined sets of curves which, with the exception that the curves for $P = 0^+$ do not have rays extending to infinity, are qualitatively very similar for all four cases. For hard squares, on the other hand, the four different plots are qualitatively different from each other and are far more complicated than those for hard hexagons.

The cylinder partition function $Z_{L,L}^{FC}(z) = Z_{L,L}^{CF}(z)$ allows a direct comparison between the equimodular curves of $T_F(z)$ and $T_{C0^+}(z)$ in figures 6 and 7, since both transfer matrices can be used to construct the same partition function. For both hard squares and hard hexagons these figures show that the zeros of the $L \times L$ cylindrical partition function lie much closer to the equimodular curves of $T_F(z)$ rather than T_{C0^+} . It is only for much larger aspect ratios that the cylinder zeros lie close to the T_{C0^+} equimodular curves, as can be seen, for example, in figure 8, where we plot the hard square $Z_{26n,26}^{FC}(z)$ roots for $n = 1, 2, 3, 4, 5, 10$ along with the $L_h = 26$ equimodular curves of $T_{C0^+}(z)$.

For hard squares, the arlike structures noted above for figure 2 are in remarkable agreement with the $T_F(z)$ curves which originate near $z = -1$ and extend to infinity. There are L_h such equimodular curves which is exactly the number of points seen above to lie on each of the arlike structures of zeros.

For hard squares both $T_C(z; L_h)$ and $T_F(z; L_h)$ shown in figure 6 have equimodular curves which extend out to $|z| = \infty$. In Appendix C we present an analytical argument that both the $T_C(z; L_h)$ and $T_F(z; L_h)$ curves have L_h branches going out to infinity at asymptotic angles $\arg z = \frac{(1+2k)\pi}{L_h}$ with $k = 0, 1, \dots, L_h - 1$.

For hard hexagons it was seen in [24] that when $L_h \equiv 0 \pmod{3}$ the curves for $T_C(z; L_h)$ as illustrated in figure 7 have $2L_h/3$ rays extending to infinity which separate regions with $P = 0^+$ from regions with $\pm 2\pi/3$. However, for the hard hexagon matrix $T_F(z; L_h)$ it is evident in figure 7 there is much more structure in the curves which extend to infinity. This is shown on a much larger scale in figure 9. This more complicated structure for the equimodular curves of $T_F(z; L_h)$ presumably results from the fact that for hard hexagons $T_F(z; L_h)$ is neither translation nor reflection invariant.

Just as for hard hexagons it is only possible for hard squares to identify an endpoint of an equimodular curve approaching z_c for the transfer matrix $T_C(z; L_h)$ in the $P = 0^+$ sector. We give the location of the $z_c(L_h)$ and $z_d(L_h)$ endpoints for $P = 0^+$ in table 2.

For hard squares the transfer matrix $T_F(z; L_h)$ with free boundary conditions is invariant under parity in contrast with hard hexagons where there is no parity invariance. The maximum eigenvalue for hard squares has positive parity and in figure 10 we compare for $L_h = 16$ the equimodular curves of $T_F(z; L_h)$ with the restriction to positive parity. We also compare the equimodular curves for $L_h = 16$ of $T_C(z; L_h)$ and its restriction to $P = 0^+$.

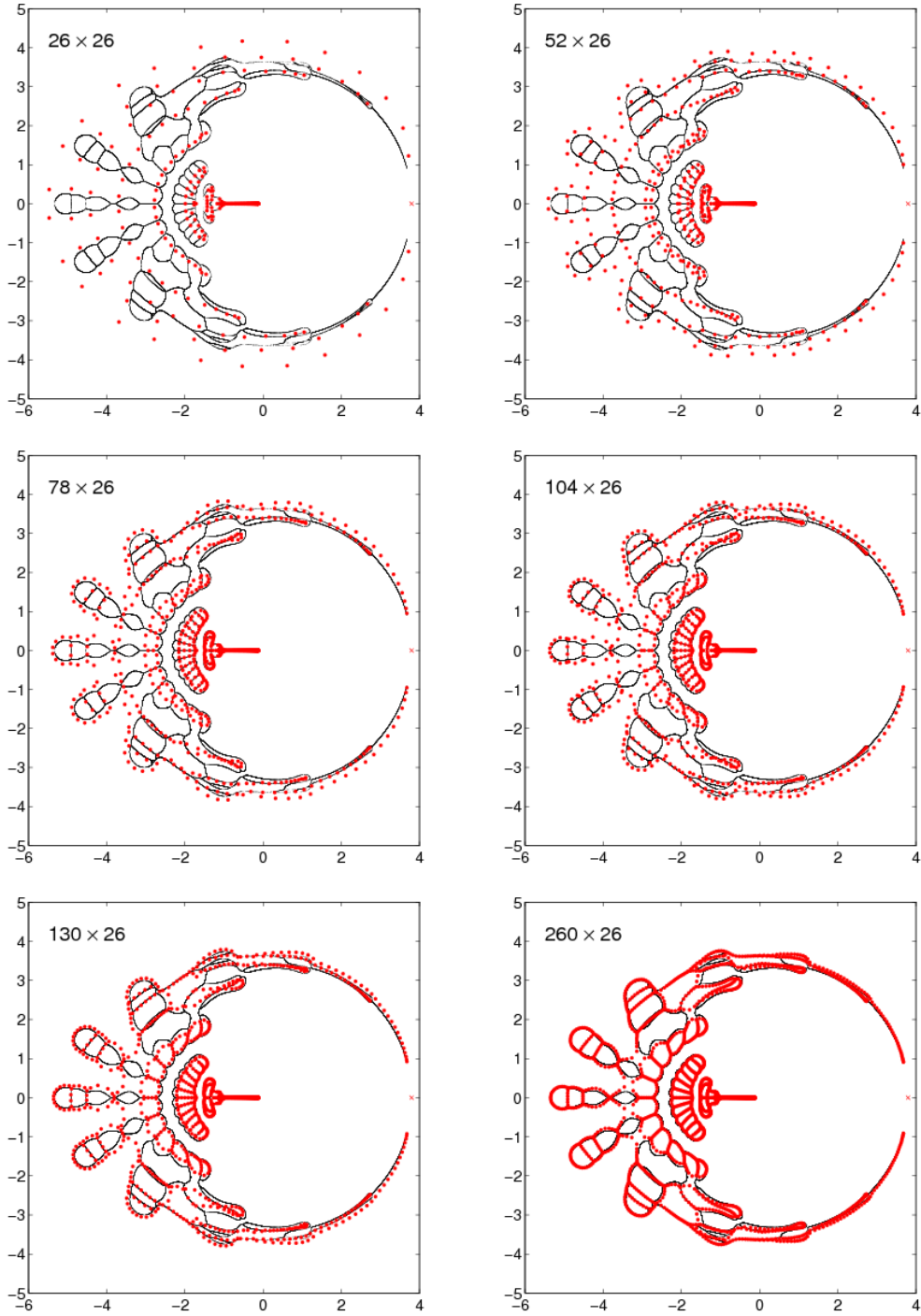


Figure 8. Plots in the complex fugacity z -plane of the zeros of the partition function $Z_{L_v, L_h}^{FC}(z)$ of hard squares for $L_v \times 26$ lattices with cylindrical boundary conditions (in red) compared with the $P = 0^+$ equimodular curves of $T_C(z; 26)$ (in black). The location of z_c is indicated by a cross.

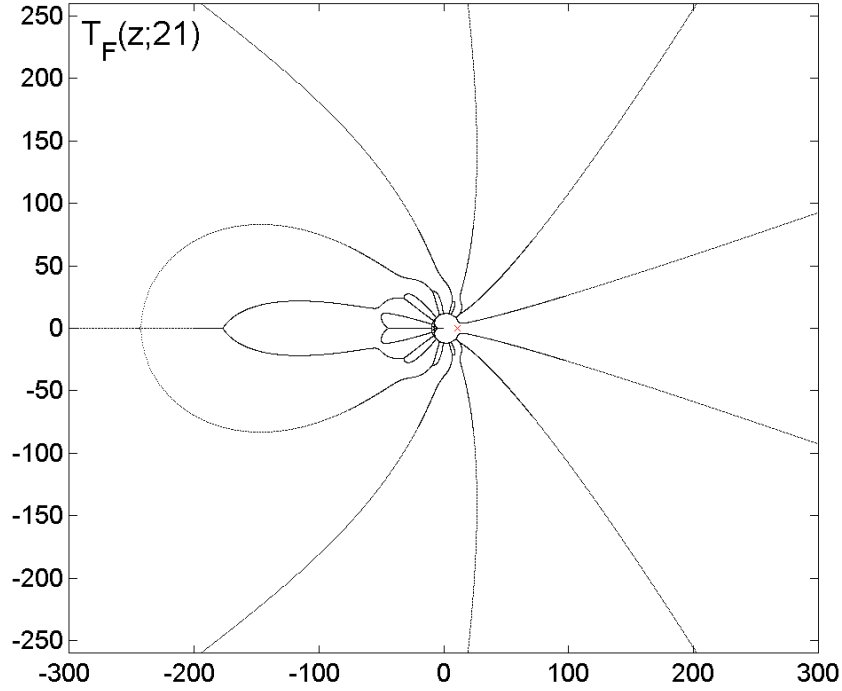


Figure 9. Equimodular curves for the hard hexagon transfer matrix $T_F(z; L_h)$ for $L_h = 21$ showing the complex structure which exists for $|z| \geq 12$. The location of z_c is indicated by a cross.

L_h	$z_c(L_h)$ endpoint	$z_d(L_h)$ endpoint
4	$-0.8806 \pm i3.4734$	-0.1259
6	$1.6406 \pm i3.2293$	-0.1216
8	$2.5571 \pm i2.6694$	-0.1204
10	$2.9955 \pm i2.2264$	-0.1200
12	$3.2374 \pm i1.8961$	-0.1197
14	$3.3845 \pm i1.6461$	-0.1196
16	$3.479 \pm i1.4547$	
18	$3.544 \pm i1.3032$	
20	$3.591 \pm i1.1780$	
22	$3.627 \pm i1.0722$	
24	$3.654 \pm i0.9841$	
26	$3.675 \pm i0.9117$	
∞	3.796255	-0.119338

Table 2. The endpoints of the equimodular curves of $T_C(z; L_h)$ with $P = 0^+$ which approach z_c and z_d as L_h increases. For $L_h \leq 14$ the endpoints are computed from the vanishing of the discriminant of the characteristic polynomial and have been computed to 50 decimal places. For $L_h \geq 16$ they are determined numerically to 3 decimal places and consequently the deviation from z_d is too small to be accurately determined.

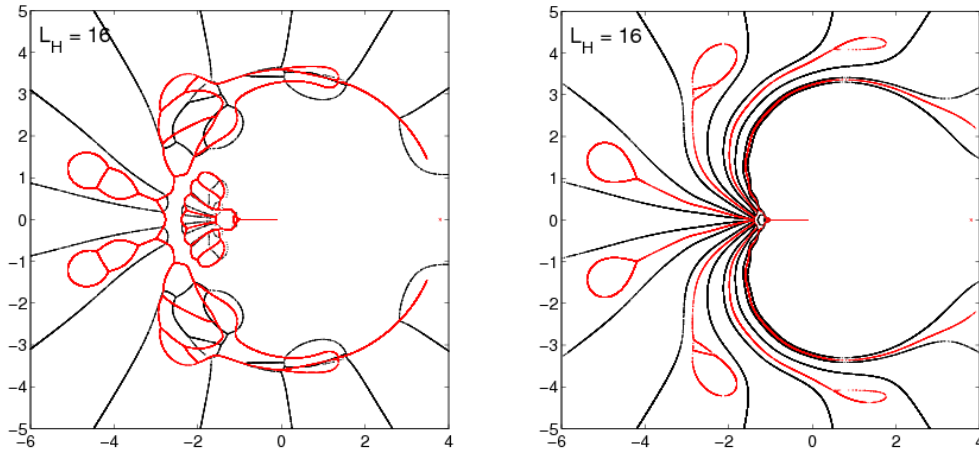


Figure 10. On the left the comparison for hard squares with $L_h = 16$ of the equimodular curves of $T_C(z; L_h)$ in black with the restriction to $P = 0^+$ in red. On the right the comparison for hard squares with $L_h = 16$ of the equimodular curves of $T_F(z; L_h)$ in black with the restriction to the positive parity sector in red. The location of z_c is indicated by a cross.

4. Comparisons on $-1 \leq z \leq z_d$

A much more quantitative comparison of hard squares and hard hexagons can be given on the interval $-1 \leq z \leq z_d$. We treat both transfer matrix eigenvalues and partition function zeros.

4.1. Transfer matrix eigenvalue gaps

The eigenvalues of the transfer matrix $T_C(z; L_h)$ for hard hexagons for $P = 0^+$ have two very remarkable properties discovered in [24]

- (i) The characteristic polynomial of $T_C(z)$ in the sector $P = 0^+$ for $L_h = 9, 12, 15, 18$ factorizes into the product of two irreducible polynomials with integer coefficients.
- (ii) The roots of the discriminant of the characteristic polynomial which lie on the real axis for $z < z_{d,hh}(L)$ all have multiplicity two for $L_h \leq 18$. In particular on the negative real axis the maximum eigenvalue is real only at isolated points. We conjecture this is valid for all L_h .

The hard hexagon transfer matrix $T_F(z; L_h)$ for $L_h = 3, 6, 9$ also has the remarkable property that all the roots of the resultant on the interval $-1 < z < z_d$ have multiplicity two. This is very strong evidence to support the conjecture that hard hexagons with free boundary conditions in one direction and cyclic in the other direction is obtained as a limit from a model which obeys the boundary Yang-Baxter equation of [32, 33].

Neither property i) nor ii) can be considered as being generic and neither property holds for hard squares where there are small gaps in the equimodular curves where the maximum eigenvalues of both $T_C(z; L_h)$ and $T_F(z; L_h)$ are real and non-degenerate.

These gaps are caused by the collision of a complex conjugate pair of eigenvalues at the boundaries of the gaps. On $-1 \leq z \leq z_d$ the maximum eigenvalue of $T_C(z; L_h)$ is in the sector $P = 0^+$. We have computed these gaps numerically for $L_h \leq 20$ and more accurately from the discriminant of the characteristic polynomial for $L_h \leq 14$. We give these gaps in table 3 for $L_h \leq 20$. For $L_h \geq 22$ most of the gaps are too small to actually observe their width, but their locations can still be determined numerically and are given in table 4 for $22 \leq L_h \leq 30$.

L_h	$z_l(L_h)$	$z_r(L_h)$	gap	eigenvalue sign
6	-0.52385422	-0.47481121	4.904301×10^{-2}	-
8	-0.30605227	-0.30360084	2.35243×10^{-3}	-
10	-0.23737268	-0.23720002	1.7266×10^{-4}	-
	-0.77929238	-0.73645527	4.283711×10^{-2}	+
12	-0.20401756	-0.20400239	1.517×10^{-5}	-
	-0.49539291	-0.49352002	1.87289×10^{-3}	+
14	-0.18464415	-0.18464265	1.50×10^{-6}	-
	-0.37193269	-0.37180394	1.2875×10^{-4}	+
	-0.92551046	-0.91949326	6.01721×10^{-3}	-
16	-0.17211444	-0.1721143	1.4×10^{-7}	-
	-0.305086	-0.305078	8×10^{-6}	+
	-0.64336	-0.64204	1.32×10^{-3}	-
18	-0.163389012	-0.163388998	1.4×10^{-8}	-
	-0.2643054	-0.2643045	9×10^{-7}	+
	-0.494482	-0.494388	9.4×10^{-5}	-
20	-0.156991031	-0.156991029	2×10^{-9}	-
	-0.23723539	-0.23723530	9×10^{-8}	+
	-0.404127	-0.494120	7×10^{-6}	-
	-0.7537	-0.7523	1.4×10^{-3}	+

Table 3. The gaps on the segment $-1 \leq z \leq z_d$ where the maximum eigenvalue of the transfer matrix $T_C(z; L_h)$ for hard squares on cylindrical chains of length L_h is real for $6 \leq L_h \leq 20$.

The gaps of $T_F(z; L_h)$ are not the same as those of $T_C(z; L_h)$. The gaps of $T_F(z; L_h)$ are given in table 5 where we see that with increasing L_h they approach the gaps of $T_C(z; L_h)$ of table 3.

The location of gaps for larger values of L_h may be extrapolated by observing that when the maximum eigenvalues λ_{\max} are complex they may be written as $|\lambda_{\max}|e^{\pm i\theta/2}$ where θ is defined in section 2.5. The eigenvalues collide and become real when θ/π is an integer. In principle each of the separate equimodular curves on $-1 \leq z \leq z_d$ could be independent of each other, but as long as we are to the right of any equimodular curve which intersects the z axis, we define by convention the eigenvalue phase at the right of a gap to be the same as the phase at the left of the gap. We then choose θ not to be restricted to the interval 0 to π but to continuously increase as z decreases from z_d to the first crossing of an equimodular curve. This convention preserves the alternation of the signs of the real eigenvalues seen in table 3. For $L_h = 6$ we illustrate the behavior of this phase in figure 11. At the boundaries of the gaps the derivative of the phase diverges as a square root, and for $L_h = 6$ this derivative is also plotted in figure 11.

L_h	1	2	3	4	5	6	7	8
22	-0.152	-0.218	-0.346	-0.598				
24	-0.148	-0.204	-0.305	-0.494	-0.844			
26	-0.145	-0.193	-0.276	-0.423	-0.683			
28	-0.143	-0.184	-0.254	-0.371	-0.574	-0.93		
30	-0.140	-0.178	-0.237	-0.334	-0.495	-0.75		
32	-0.1388	-0.172	-0.223	-0.305	-0.435	-0.642	-0.972	
34	-0.1373	-0.167	-0.213	-0.282	-0.390	-0.558	-0.815	
36	-0.1360	-0.163	-0.204	-0.264	-0.355	-0.494	-0.701	
38	-0.1348	-0.160	-0.196	-0.249	-0.327	-0.444	-0.616	-0.871
40	-0.1338	-0.157	-0.190	-0.237	-0.305	-0.405	-0.548	-0.752

Table 4. The location of the very small gaps on the segments $-1 \leq z \leq z_d$ where the maximum eigenvalue of the transfer matrix $T_C(z; L_h)$ for hard squares is real. For $L_h = 22, 24, 26, 28, 30$ the values are obtained from the data; for $L_h \geq 32$ the values are obtained from extrapolation using figure 12.

L_h	$z_l(L_h)$	$z_r(L_h)$	gap	eigenvalue sign
6	-0.4517	-0.4439	7.8×10^{-3}	-
8	-0.3004	-0.2999	5×10^{-4}	-
10	-0.23987	-0.23983	4×10^{-5}	-
	-0.6933	-0.6868	6.6×10^{-3}	+
12	-0.2079551	-0.2079504	4.6×10^{-6}	-
	-0.46977	-0.46908	6.9×10^{-4}	+
14	-0.18864888	-0.8864835	5.3×10^{-7}	-
	-0.362749	-0.362722	2.7×10^{-5}	+
	-0.85376	-0.85315	6.1×10^{-4}	-
16	-0.175819604	-0.175819540	6.4×10^{-8}	-
	-0.3024077	-0.3024052	2.5×10^{-6}	+
	-0.61069	-0.61049	2.0×10^{-4}	-

Table 5. The gaps on the segment $-1 \leq z \leq z_d$ where the maximum eigenvalue of the transfer matrix $T_F(z; L_h)$ for hard squares on the free chain of length L_h is real for $6 \leq L_h \leq 16$.

For any given value of z this unrestricted phase grows linearly with L_h and thus we define a normalized phase

$$\phi = \frac{\theta}{2\pi L_h}. \quad (46)$$

The gaps occur when $L_h \phi = 1$. In figure 12 we plot the normalized phases ϕ_C of $T_C(z; L_h)$ for $4 \leq L_h \leq 26$ and observe that they fall remarkably close to a common limiting curve. We may thus use this curve to extrapolate the locations of the gaps for $L_h \geq 32$. These values are given in table 4 for $32 \leq L_h \leq 40$. We also plot in figure 12 the normalized phase ϕ_F for $T_F(z; L_h)$ and note that $\phi_F \rightarrow \phi_C$ as L_h becomes large.

4.2. The density of partition zeros of $L \times L$ lattices on the negative z axis

For both hard squares and hard hexagons the zeros on the negative real axis are sufficiently dense that a quantitative comparison in terms of a density is possible.

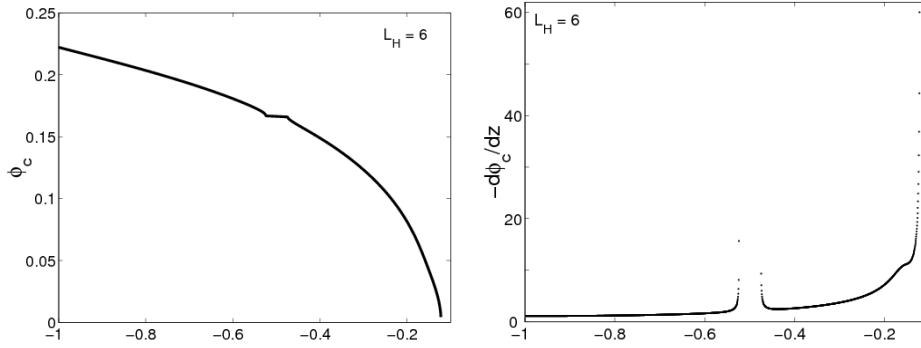


Figure 11. The normalized phase $\phi_C(z)$ of the equimodular curve of $T_C(z; L_h)$ and the derivative $-d\phi_C(z)/dz$ for $L_h = 6$ which has one gap on $-1 \leq z \leq z_d$ where λ_{\max} is real.

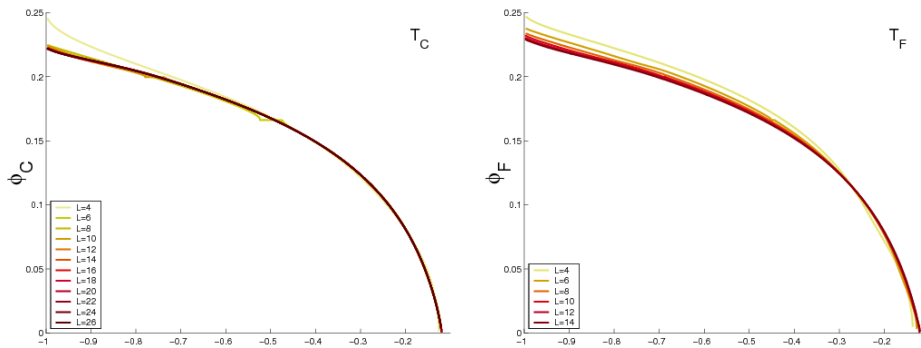


Figure 12. The normalized phase angles ϕ_C of $T_C(z; L_h)$ (on the left) and ϕ_F of $T_F(z; L_h)$ (on the right) on the segment $-1 \leq z \leq z_d$ as a function of z .

The density of partition function zeros on $L_v \times L_h$ lattices with L_v/L_h fixed and $L_v, L_h \rightarrow \infty$ is the limit of the finite lattice quantity

$$\tilde{D}_{L_v, L_h}(z_j) = \frac{1}{L_v L_h (z_{j+1} - z_j)} > 0 \quad (47)$$

and the positions of the zeros z_j increase monotonically with j . To analyze this density we will also need the n^{th} order lattice derivative

$$\tilde{D}_{L_v, L_h}^{(n)}(z_j) = \frac{\tilde{D}_{L_v, L_h}^{(n-1)}(z_{j+1}) - \tilde{D}_{L_v, L_h}^{(n-1)}(z_j)}{z_{j+1} - z_j}. \quad (48)$$

As long as the density on $-1 \leq z \leq z_d$ is the boundary of the zero free region which includes the positive real axis (and where the thermodynamic limiting free energy is independent of the aspect ratio L_v/L_h), the limiting density computed directly for the $L_v \times L_h$ lattice is given in terms of the normalized phase angle (46) $\phi(z)$ on the

interval $-1 \leq z \leq z_d$ by use of (37) as

$$\lim_{L_h, L_v \rightarrow \infty} \tilde{D}_{L_v, L_h}(z) = - \lim_{L_h \rightarrow \infty} \frac{d\phi(z)}{dz}. \quad (49)$$

Partition function zeros have been computed for systems much larger than it has been possible to compute eigenvalues and the largest lattices are for the $L \times L$ cylinders. In figure 13 we plot the density and the first three lattice derivatives for hard squares for the 40×40 cylindrical lattice on $-1 \leq z \leq z_d$. On this scale the density appears to be quite smooth and a local maximum is seen in the first derivative.

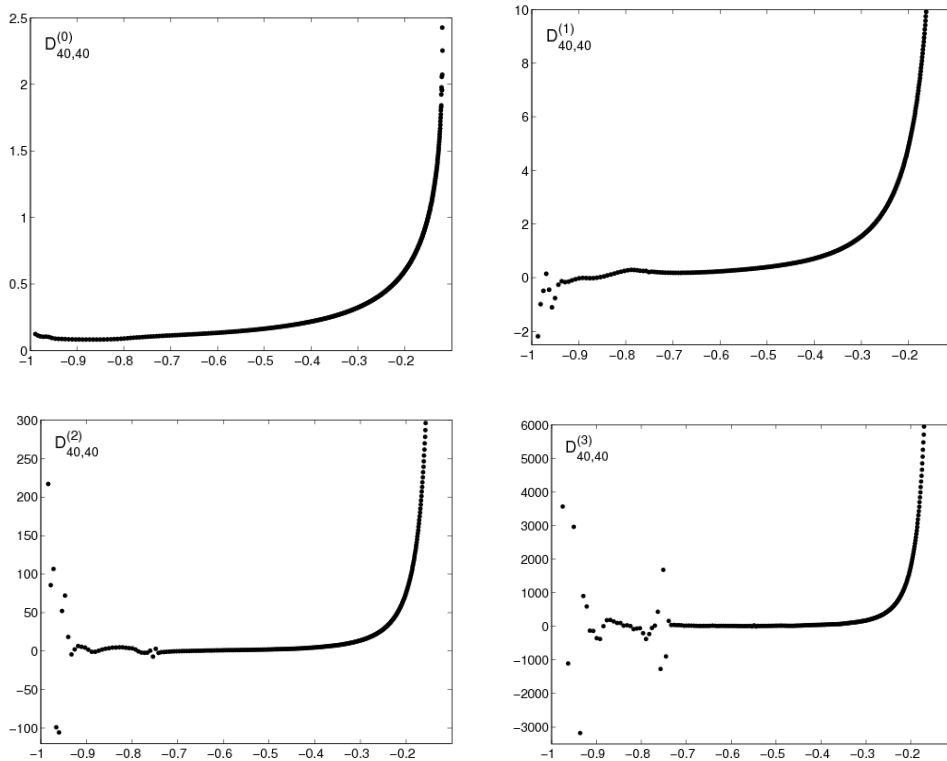


Figure 13. The density of zeros and the first three lattice derivatives for hard squares for the 40×40 lattice with cylindrical boundary conditions in the region $-1 \leq z \leq z_d$. The glitch, defined in section 4.4, caused by the gap given in table 4 at $z = -0.752$ is clearly visible in the second and third derivatives.

4.3. Partition zeros versus phase derivatives

For hard hexagons the density of partition function zeros on the negative z axis lie very close to the density computed from the derivative of the phase angle (49). Moreover all the lattice derivatives are smooth and featureless except very near $z_{d;hh}$ and also agree remarkably well with the derivatives computed from the phase angle. This is in significant contrast to hard squares.

In figure 14 we compare the density of zeros and its first two lattice derivatives with the same quantities computed from the normalized phase derivative curves of the corresponding transfer matrix for the 22×22 toroidal lattice and the 14×14 cylindrical lattice. For the density almost all zeros are seen to fall remarkably close to the normalized phase derivative curves. In the first derivative of the normalized phase derivative curve we see the divergences due to the gaps at -0.60 for $T_C(z; 22)$ and at -0.85 and -0.36 for $T_F(z; 14)$. In the second derivative, the divergences become more pronounced and the gap at -0.35 of $T_C(z; 22)$ becomes noticeable.

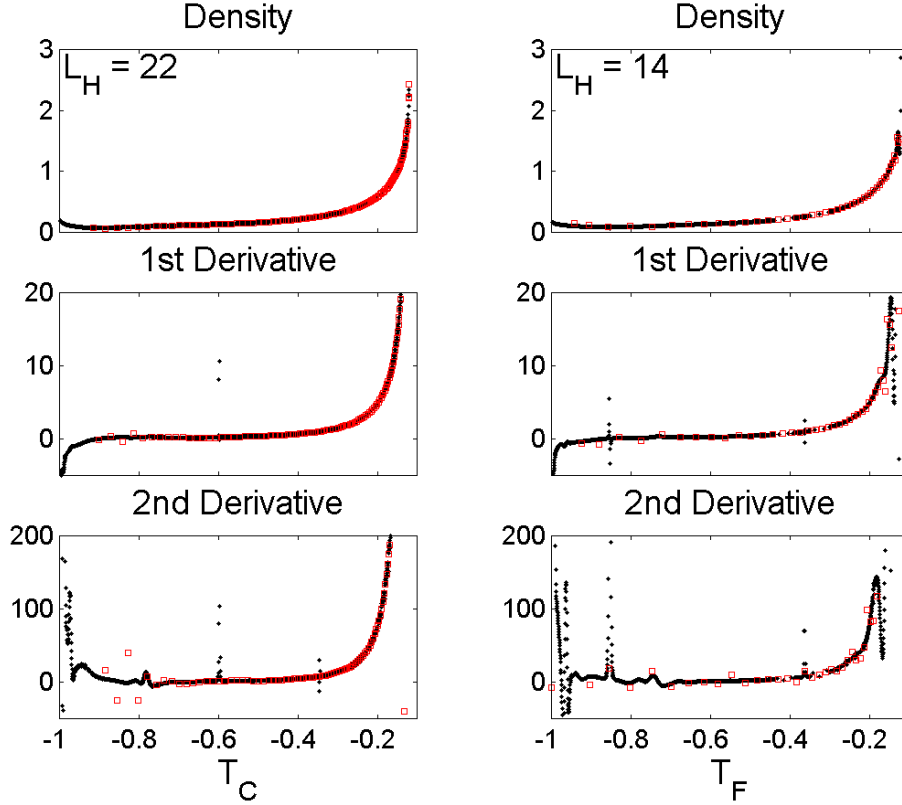


Figure 14. The density and the first two derivatives of the partition function zeros (in red) compared with the derivatives of the normalized phase derivative curves (in black) of the toroidal lattice $Z_{22,22}^{CC}(z)$ for the $T_C(z; 22)$ on the left and the zeros of $Z_{14,14}^{CF}(z) = Z_{14,14}^{FC}(z)$ cylinder and the $T_F(z; 14)$ transfer matrices (on the right). The divergences due to the gaps at $z = -0.598, -0.346$ for $T_C(z; 22)$ and at $z = -0.853, -0.3627$ for $T_F(z; 14)$ can be seen.

The derivatives of the normalized phase derivative curves all exhibit oscillations in the vicinity of $z = -1$ which become larger and cover an increasing segment of the z axis as the order of the derivative increases. In these oscillatory regions noticeable discrepancies between the lattice derivative of the zeros and the derivatives of the normalized phase are apparent.

4.4. Glitches in the density of zeros

The gaps in the equimodular curves of hard squares on $-1 \leq z \leq z_d$ which caused the divergences in the normalized phase curves in figure 14 lead to irregularities in the density of the $L \times L$ partition function zeros which we refer to as “glitches”. These glitches upset the smoothness of the density of zeros on the finite lattice and become increasingly apparent in the higher derivatives of the density. The glitch at $z = -0.752$ is quite visible in the second and third derivatives in figure 13.

To illustrate further the relation of gaps to glitches in the density of zeros we plot the third derivatives of the density of cylindrical $L \times L$ lattices on an expanded scale in figure 15 where we indicate with solid arrows the positions of the corresponding gaps in the $T_C(z; L_h)$ equimodular curves of table 4. On these expanded scales we observe that as the size of the $L \times L$ lattice increases the number of glitches increases, they move to the right and their amplitude decreases. These properties follow from the properties of the gaps of table 4 and the normalized phase curve of figure 12.

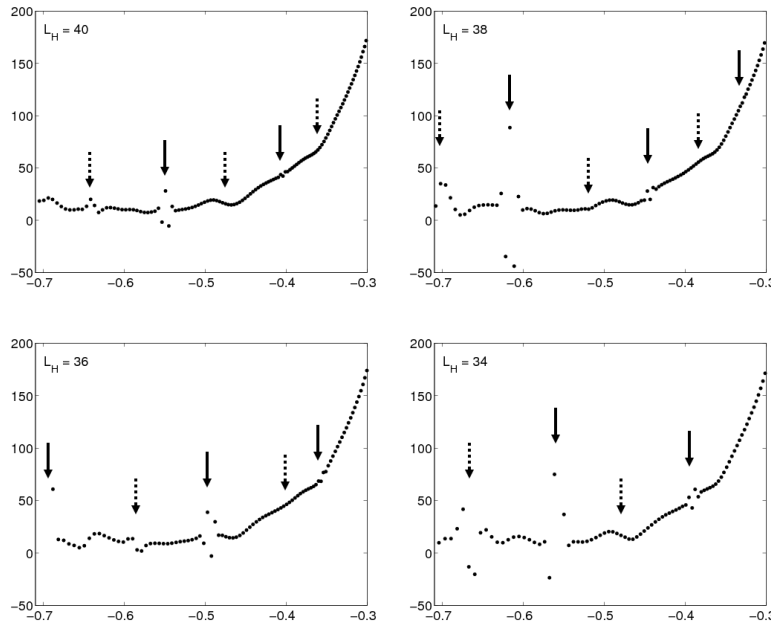


Figure 15. The third derivative of the density of hard squares for 40×40 , 38×38 , 36×36 , 34×34 lattices with cylindrical boundary conditions in the region $-0.7 \leq z \leq -0.25$. The gaps of table 4 are indicated by solid arrows

There also appear to be deviations of the zeros from a smooth curve at values of z where the phases of the complex conjugate pair of maximum modulus eigenvalues are $\pm\pi/2$. These deviations have no relation to gaps in the equimodular curves and are indicate with dashed arrows in figure 15.

4.5. Hard square density of zeros for $z \rightarrow z_d$.

As $z \rightarrow z_d$ the density diverges as

$$D(z) \sim (z_d - z)^{-\alpha}, \quad (50)$$

where from the universality of the point z_d with the Lee-Yang edge it is expected that $\alpha = 1/6$, which was also found to be the case for hard hexagons. We investigate the exponent α using the method used in [24] by plotting in figure 16 the quantity $D_L(z)/D_L^{(1)}(z)$ for $L = 40$ and compare this with

$$D(z)/D'(z) \sim (z_d - z)/\alpha \quad \text{with } \alpha = 1/6, \quad (51)$$

which is expected to hold for $z \rightarrow z_d$.

As was the case for hard hexagons this limiting form is seen to hold only for z very close to z_d and for comparison we also plot a fitting function

$$f(z) = (z_f - z)/\alpha_f \quad \text{with } z_f = -0.058, \quad \alpha_f = 1/0.88, \quad (52)$$

which well approximates the curve in the range $-0.30 \leq z \leq -0.16$. This same phenomenon has been seen in [44, equation (4.8) and figure 41] for Hamiltonian chains.

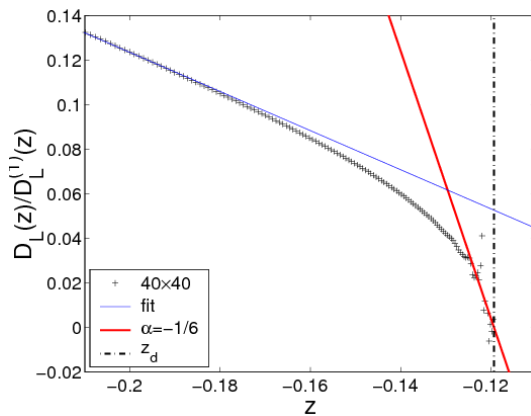


Figure 16. The plot of density/derivative for the partition function zeros of hard squares for 40×40 cylindrical lattice. The red line has $\alpha = 1/6$ and $z_d = -0.119$. The blue line has $\alpha_f = 1/0.88 = 1.14$ and $z_f = -0.058$.

4.6. The point $z = -1$

Hard squares have the remarkable property, which has no counterpart for hard hexagons, that at $z = -1$ all roots of the characteristic equation are either roots of one, or minus one, with various multiplicities. These roots have been computed for the full transfer matrix $T_C(-1; L_h)$ either directly [18], [23] to size 15 or using a mapping to rhombus tilings [19] to size $L_h = 50$. In Appendix A we present factorizations of the characteristic polynomial $T_C(-1; L_h)$ for the reduced sector $P = 0^+$ for $L_h \leq 29$, and of $T_F(-1; L_h)$ for $L_h \leq 20$ both for the unrestricted and positive parity sectors. In Appendix B we give the partition function values at $z = -1$.

4.7. Behavior near $z = -1$

The density of zeros of figure 13 for the 40×40 cylinder is finite as $z \rightarrow -1$. However the first derivative is sufficiently scattered for $z \leq -0.95$ that an estimate of the slope is impracticable.

Furthermore there is a great amount of structure in the equimodular curves near the point $z = -1$ where all eigenvalues are equimodular and which is not apparent

on the scale of the plots in figure 6. We illustrate this complexity for $L_h = 12$ for $P = 0^+$ in figure 17 where we see that there are equimodular curves which intersect the z axis for $z \geq -1$. These level crossings are a feature also for $T_C(z)$ without the restriction to $P = 0^+$ and for $T_F(z)$ and $T_F(z)$ with $+$ parity as well. In general there are several such crossings for a given L_h . We give the values of the crossing furthest to the right in table 6. It is not clear whether these level crossings will persist to the right of $z = -1$ as $L_h \rightarrow \infty$. We also note that often there are more than one such level crossing, as illustrated in figure 17 for $T_F(z; 12)$.

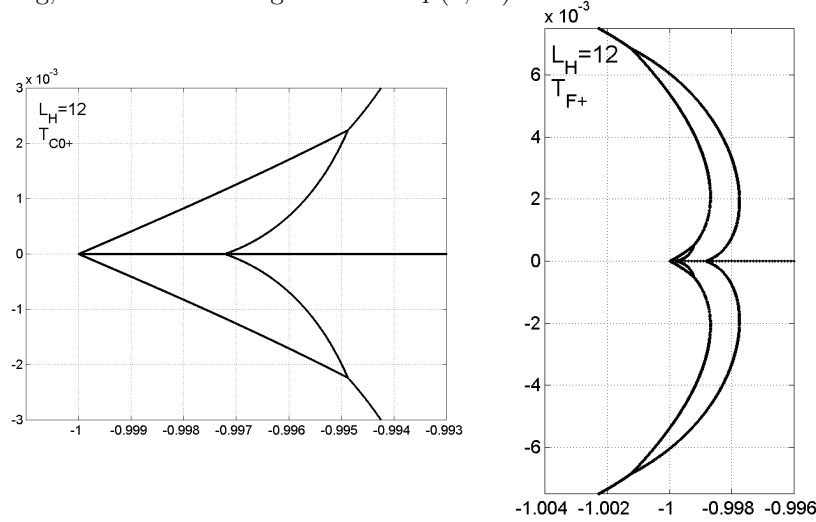


Figure 17. Plots in the complex fugacity z plane near $z = -1$ for $L_h = 12$ of the equimodular curves of hard square transfer matrix $T_C(z; L_h)$ with $P = 0^+$ (on the left) and $T_F(z; L_h)$ with $+$ parity (on the right) on a scale which shows the level crossings on the z -axis to the right of $z = -1$.

L	$P = 0^+$	T_C	parity = +	T_F
12	-0.9973	-0.91295	-0.9988	same
14	none	-0.9195	-0.999296	-0.999092
16	none	-0.96	none	none
18	-0.99994		-0.9990	
20	-0.9995			
22	-0.9999			
24	-0.9974			
26	-0.9990			
28	-0.9996			

Table 6. Positions of the right-most equimodular curve crossings of the negative z -axis for hard squares of $T_C(z)$ in the sector $P = 0^+$ and unrestricted and of $T_F(z)$ in the plus parity sector and unrestricted.

5. Discussion

The three different techniques of series expansions, transfer matrix eigenvalues and partition function zeros give three quite different perspectives on the difference between the integrable hard hexagon model and non-integrable hard squares.

5.1. Series expansions

Consider first the series expansion of the physical free energy of hard squares [13, 17], which is analyzed by means of differential approximants, as compared with the exact solution of hard hexagons [6].

The hard hexagon free energy for both the high and low density regimes satisfies Fuchsian differential equations which can be obtained from a finite number of terms in a series expansion [24].

For an non-integrable model like hard squares, the best kind of differential approximant analysis to be introduced is not clear. For integrable models, even if one has a small number of series coefficients, restricting to Fuchsian ODEs has been seen to be an extremely efficient constraint. However for a (probably non-integrable) model like hard squares, there is no reason to restrict the linear differential equations annihilating the hard square series to be Fuchsian. In [17] the existing 92 term series are analyzed by means of differential approximants but the series is too short to determine whether $z = -1$ is, or is not, a singular point.

The method of series expansions and differential approximants are not well adapted to analyze qualitative differences between hard squares and hard hexagons. This is to be compared with the transfer matrix eigenvalues and partition function zeros presented above which show dramatic differences between the two systems.

5.2. Transfer matrices

The clearest distinction between integrable hard hexagons and non-integrable hard squares is seen in the factorization properties of the discriminant of the characteristic polynomials of the transfer matrices $T_C(z; L_h)$ and $T_F(z; L_h)$. At the zeros of the discriminant the transfer matrix in general fails to be diagonalizable and the eigenvalues may have singularities.

For hard hexagons these discriminants contain square factors which exclude the existence of gaps in the equimodular curves and singularities of the maximum eigenvalue on the negative z -axis. This was observed for $T_C(z; L_h)$ in [24]. In the present paper these square factors and lack of gaps has been observed for the transfer matrix $T_F(z; L_h)$ of hard hexagons for all value of L_h studied and supports the conjecture that integrability can be established by extending the methods of [32]-[35]. For hard squares there are no such factorizations, so that its equimodular curves have gaps and the maximum eigenvalue has singularities on the negative real z -axis.

5.3. Partition function zeros

In [24] we qualitatively characterized the partition function zeros as either being on curves or being part of a necklace, and in the present paper we have characterized the zeros as filling up areas. However, further investigation is required to determine if these characterizations of the qualitative appearance of zeros of the finite system characterize the thermodynamic limit. In [24] we initiated such a study by examining

the dependence of the right-hand endpoints of the necklace on the size of the lattice and observed that the endpoints move to the right as the lattice size increases. However, there is not sufficient data to reliably determine the limiting behavior. Thus, if in the thermodynamic limit the endpoint moved to $z_{c;hh}$ the notion of zeros being on a curve might not persist. Similarly, it needs further investigation to determine if the zeros of hard squares, which we have characterized as filling up an area, will fill the area in the thermodynamic limit or whether further structure develops.

On the negative z -axis both hard hexagons and hard squares have a line of zeros which has been investigated in detail in section 4. The density of zeros for $z < z_{d;hh}$ for hard hexagons is mostly featureless and smooth, which is quite consistent with the low density free energy having a branch cut starting at $z_{d;hh}$. Hard squares zeros, on the other hand, have a series of “glitches” whose number increases as z approaches z_d and which correspond to the locations of the gaps in the equimodular curves. A rigorous analysis of behavior of these glitches needs to be made.

5.4. Behavior near z_c

The equimodular curves of hard hexagons were extensively studied in [24]. The equimodular curves, as illustrated for $L_h = 21$ in figure 7, consist of the curve where the low and high density physical free energy are equimodular and a necklace region which surrounds this equimodular curve in part of the left half-plane.

For hard hexagons there is only one unique curve of zeros of the $L \times L$ partition function which is converging towards $z_{c;hh}$ as $L \rightarrow \infty$. However, for hard squares the partition function zeros in figures 2-4 do not lie on a single unique curve near z_c . This is clearly seen in the plots of figure 5 where the zeros appear to be converging to a wedge behavior as $L \rightarrow \infty$ which is analogous to the behavior of the equimodular curves of figure 18.

The behavior of the equimodular curves of hard squares near z_c in figure 6 is qualitatively different from the behavior of hard hexagons in figure 7. This is vividly illustrated in figure 18 where we plot the equimodular curves for $T_c(z; L_h)$ with $P = 0^+$ for all values $4 \leq L_h \leq 26$. We see in this figure that there is an ever increasing set of loops in the equimodular curves which approach z_c as $L_h \rightarrow \infty$.

It needs to be investigated if this behavior of both the zeros and the equimodular curves for hard squares will have an effect on the singularity at z_c beyond what is obtained from the analysis of the series expansion of [13, 17].

5.5. Behavior near $z = -1$

Finally we note that the relation of the equimodularity of all eigenvalues at $z = -1$ to the analytic behavior of the physical free energy is completely unknown, as is the curious observation for $12 \leq L_h \leq 28$ found in table 6 that there are equimodular curves of $T_C(z; L_h)$ and for $T_F(z; L_h)$ which cross the negative z -axis to the right of $z = -1$. There are many values of L_h for which there are more than one such curve. It would be of interest to know if this feature persists for $L_h > 28$ and if it does, does the point of rightmost crossing move to the right. If such a phenomenon does exist it would cause a re-evaluation of the role of zeros on the negative z -axis.

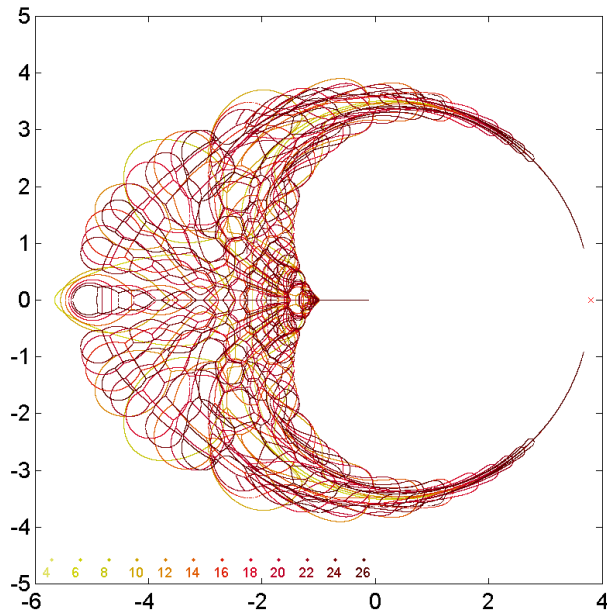


Figure 18. The equimodular curves in the complex z plane of the $T_C(z; L_h)$ transfer matrix in the 0^+ sector for $4 \leq L_h \leq 26$ plotted together. The different values of L_h are given different shadings as indicated on the plot. The location of z_c is indicated by a cross.

6. Conclusions

The techniques of series expansions, universality and the renormalization group apply equally well to describe the dominant behavior at z_c and z_d of hard hexagons and hard squares. However the results of this paper reveal many differences between integrable hard hexagons and non-integrable hard squares which have the potential to create further analytic properties in hard squares which are not present in hard hexagons.

The renormalization group combined with conformal field theory predicts that both z_c and z_d will be isolated regular singularities where the free energy will have a finite number of algebraic or logarithmic singularities, each multiplied by a convergent infinite series. This scenario is, of course, far beyond what can be confirmed by numerical methods. Indeed hard squares are predicted to have the same set of 5 exponents at z_d which hard hexagons have [36],[24] even though only two such exponents can be obtained from the 92 terms series expansion [17].

The emergence of the critical singularities predicted by the renormalization group at either z_c or z_d is a phenomenon which relies upon the thermodynamic limit and we have seen that hard squares approach this limit in a more complicated manner than do hard hexagons.

Near z_c the limiting position of the zeros for hard squares appears to be a wedge. This is far more complex than the behavior of hard hexagons.

Near z_d the zeros of both hard hexagons and hard squares are observed to lie on a segment of the negative z -axis. If this indeed holds in the thermodynamic limit it

would be satisfying if a genuine proof could be found which incorporates the fact that some level crossings have been observed to the right of $z = -1$.

On the negative z -axis hard squares have glitches in the density of zeros and gaps in the equimodular curves which hard hexagons do not have. In the thermodynamic limit the glitches and gaps may become a dense set of measure zero by the analysis leading to table 4 . Does this give a hint of the analytical structure of non-integrable models?

Acknowledgments

We are pleased to acknowledge fruitful discussions with C. Ahn, A.J. Guttmann, and P.A. Pearce. One of us (JJ) is pleased to thank the Institut Universitaire de France and Agence Nationale de la Recherche under grant ANR-10-BLAN-0401 and the Simons Center for Geometry and Physics for their hospitality. One of us (IJ) was supported by an award under the Merit Allocation Scheme of the NCI National facility at the ANU and by funding under the Australian Research Council's Discovery Projects scheme by the grant DP140101110. We also made extensive use of the High Performance Computing services offered by ITS Research Services at the University of Melbourne.

Appendix A. Characteristic polynomials at $z = -1$

In [19] it was proven that all of the eigenvalues of the $T_C(-1; L_h)$ transfer matrix at $z = -1$ are roots of unity and the characteristic polynomials were given in that paper up to $L_h = 50$. Below we give the factorized characteristic polynomials $P_{L_h}^{C0+}$ in the 0^+ sector at $z = -1$ up to $L_h = 29$. The transfer matrix $T_F(z; L_h)$ has not been considered before in the literature, and below we give the factorized characteristic polynomials $P_{L_h}^F$ and $P_{L_h}^{F+}$ of the full $T_F(-1; L_h)$ and the restricted positive parity sector, respectively, at $z = -1$ up to $L_h = 20$. In all cases divisions are exact.

Appendix A.1. Characteristic polynomials $P_{L_h}^F$

The degree of $P_{L_h}^F$ is exactly the Fibonacci number $F(n)$ defined by the recursion relation

$$F(L_h + 2) = F(L_h + 1) + F(L_h) \quad (\text{A.1})$$

with the initial conditions $F(-1) = 0$, $F(0) = 1$, so that its generating function is

$$G^F = \frac{(2+t)}{(1-t-t^2)} \quad (\text{A.2})$$

and thus as $L_h \rightarrow \infty$ the degree of the polynomial $P_{L_h}^F$ grows as $N_G^{L_h}$, where $N_G = (1 + \sqrt{5})/2 \sim 1.618 \dots$ is the golden ratio.

The first 20 polynomials are

$$\begin{aligned} P_1^F &= (x^6 - 1)(x^3 - 1)^{-1}(x^2 - 1)^{-1}(x - 1) \\ P_2^F &= (x^4 - 1)(x^2 - 1)^{-1}(x - 1) \\ P_3^F &= (x^8 - 1)(x^4 - 1)^{-1}(x - 1) \\ P_4^F &= (x^6 - 1)(x^4 - 1)(x^3 - 1)^{-1}(x - 1) \\ P_5^F &= (x^{10} - 1)(x^8 - 1)/(x^4 - 1)(x^2 - 1)^{-1}(x - 1) \end{aligned}$$

$$\begin{aligned}
P_6^F &= (x^{14} - 1)(x^4 - 1)^2(x^2 - 1)^{-1}(x - 1) \\
P_7^F &= (x^{18} - 1)(x^{12} - 1)(x^8 - 1)(x^6 - 1)(x^4 - 1)^{-2}(x^3 - 1)^{-1}(x - 1) \\
P_8^F &= (x^{22} - 1)(x^{16} - 1)^2(x^8 - 1)^{-1}(x^4 - 1)^2(x - 1) \\
P_9^F &= (x^{26} - 1)(x^{20} - 1)^3(x^{14} - 1)(x^{10} - 1)^{-1}(x^8 - 1)(x^4 - 1)^{-2}(x^2 - 1)^{-1}(x - 1) \\
P_{10}^F &= (x^{30} - 1)(x^{24} - 1)^3(x^{18} - 1)^2(x^8 - 1)^{-1}(x^6 - 1)(x^4 - 1)^3(x^3 - 1)^{-1} \\
&\quad (x^2 - 1)^{-1}(x - 1) \\
P_{11}^F &= (x^{34} - 1)(x^{28} - 1)^3(x^{22} - 1)^4(x^{16} - 1)(x^{14} - 1)(x^8 - 1)(x^4 - 1)^{-3}(x - 1) \\
P_{12}^F &= (x^{38} - 1)(x^{32} - 1)^4(x^{26} - 1)^6(x^{20} - 1)^2(x^{10} - 1)(x^8 - 1)^{-1}(x^4 - 1)^3(x - 1) \\
P_{13}^F &= (x^{42} - 1)(x^{36} - 1)^5(x^{30} - 1)^8(x^{24} - 1)^5(x^{12} - 1)(x^{10} - 1)(x^8 - 1)^2(x^6 - 1) \\
&\quad (x^4 - 1)^{-3}(x^3 - 1)^{-1}(x^2 - 1)^{-1}(x - 1) \\
P_{14}^F &= (x^{46} - 1)(x^{40} - 1)^5(x^{34} - 1)^{11}(x^{28} - 1)^{11}(x^{22} - 1)^3(x^{14} - 1)^{-1}(x^8 - 1)^{-1} \\
&\quad (x^4 - 1)^4(x^2 - 1)^{-1}(x - 1) \\
P_{15}^F &= (x^{50} - 1)(x^{44} - 1)^5(x^{38} - 1)^{14}(x^{32} - 1)^{18}(x^{26} - 1)^8(x^{22} - 1)(x^{20} - 1) \\
&\quad (x^{16} - 1)^{-2}(x^8 - 1)^2(x^4 - 1)^{-4}(x - 1) \\
P_{16}^F &= (x^{54} - 1)(x^{48} - 1)^6(x^{42} - 1)^{17}(x^{36} - 1)^{25}(x^{30} - 1)^{17}(x^{24} - 1)^4(x^{18} - 1)(x^{14} - 1) \\
&\quad (x^{12} - 1)^{-1}(x^{10} - 1)^{-1}(x^8 - 1)^{-1}(x^6 - 1)(x^4 - 1)^4(x^3 - 1)^{-1}(x - 1) \\
P_{17}^F &= (x^{58} - 1)(x^{52} - 1)^7(x^{46} - 1)^{21}(x^{40} - 1)^{35}(x^{34} - 1)^{31}(x^{28} - 1)^{11}(x^{26} - 1)^{-1} \\
&\quad (x^{22} - 1)(x^{20} - 1)^3(x^{14} - 1)^{-1}(x^{10} - 1)^{-1}(x^8 - 1)^2(x^4 - 1)^{-4}(x^2 - 1)^{-1} \\
&\quad (x - 1) \\
P_{18}^F &= (x^{62} - 1)(x^{56} - 1)^7(x^{50} - 1)^{25}(x^{44} - 1)^{50}(x^{38} - 1)^{52}(x^{32} - 1)^{24}(x^{26} - 1)^4 \\
&\quad (x^{22} - 1)^{-1}(x^{16} - 1)^2(x^8 - 1)^{-2}(x^4 - 1)^5(x^2 - 1)^{-1}(x - 1) \\
P_{19}^F &= (x^{66} - 1)(x^{60} - 1)^7(x^{54} - 1)^{29}(x^{48} - 1)^{67}(x^{42} - 1)^{82}(x^{36} - 1)^{50}(x^{30} - 1)^{14} \\
&\quad (x^{24} - 1)^{-2}(x^{18} - 1)^3(x^{14} - 1)^{-1}(x^{12} - 1)(x^{10} - 1)(x^8 - 1)^2(x^6 - 1) \\
&\quad (x^4 - 1)^{-5}(x^3 - 1)^{-1}(x - 1) \\
P_{20}^F &= (x^{70} - 1)(x^{64} - 1)^8(x^{58} - 1)^{34}(x^{52} - 1)^{84}(x^{46} - 1)^{122}(x^{40} - 1)^{97}(x^{34} - 1)^{35} \\
&\quad (x^{28} - 1)^4(x^{26} - 1)(x^{20} - 1)^{-3}(x^{14} - 1)(x^{10} - 1)(x^8 - 1)^{-2}(x^4 - 1)^5 \\
&\quad (x - 1) \tag{A.3}
\end{aligned}$$

and from these we see that the degrees of the multiplicity of the eigenvalue +1 are

$$1, 1, 1, 2, 1, 3, 2, 5, 3, 8, 9, 17, 20, 33, 45, 74, 105, 167, 250, 389, \dots \tag{A.4}$$

where we find a “mod 4” effect.

Appendix A.2. Characteristic polynomials $P_{L_h}^{F+}$

The degrees of $P_{L_h}^{F+}$ follow the sequence A001224 in the OEIS [45] and they are related to the Fibonacci sequence $F(n)$ as follows:

$$\frac{F(L_h + 1) + F(\frac{L_h + 1}{2} + 1)}{2}, \quad L_h = \text{odd} \tag{A.5}$$

$$\frac{F(L_h + 1) + F(\frac{L_h}{2})}{2}, \quad L_h = \text{even} \tag{A.6}$$

This sequence has the following generating function

$$G^{F+} = \frac{G^F}{2} + \frac{t^3 + t^2 + t + 2}{2(1 - t^2 - t^4)} \quad (\text{A.7})$$

so that the degree of the polynomials $P_{L_h}^{F+}$ grow as $N_G^{L_h}$ with a sub-dominant growth of $N_G^{L_h/2}$.

The first 20 polynomials are

$$\begin{aligned} P_1^{F+} &= (x^6 - 1)(x^3 - 1)^{-1}(x^2 - 1)^{-1}(x - 1) \\ P_2^{F+} &= (x^4 - 1)(x^2 - 1)^{-1} \\ P_3^{F+} &= (x^8 - 1)(x^4 - 1)^{-1} \\ P_4^{F+} &= (x^6 - 1)(x^3 - 1)^{-1}(x^2 - 1) \\ P_5^{F+} &= (x^8 - 1)(x^5 - 1)(x^4 - 1)^{-1} \\ P_6^{F+} &= (x^7 - 1)(x^4 - 1)^2(x^2 - 1)^{-2}(x - 1) \\ P_7^{F+} &= (x^{18} - 1)(x^9 - 1)^{-1}(x^8 - 1)(x^6 - 1)^2(x^4 - 1)^{-1}(x^3 - 1)^{-1}(x^2 - 1)^{-1} \\ &\quad (x - 1) \\ P_8^{F+} &= (x^{22} - 1)(x^{16} - 1)^2(x^{11} - 1)^{-1}(x^8 - 1)^{-2}(x^2 - 1)(x - 1) \\ P_9^{F+} &= (x^{20} - 1)^3(x^{14} - 1)(x^{13} - 1)(x^{10} - 1)^{-3}(x^8 - 1)(x^7 - 1)^{-1}(x^4 - 1)^{-2} \\ &\quad (x - 1) \\ P_{10}^{F+} &= (x^{18} - 1)^2(x^{15} - 1)(x^{12} - 1)^3(x^9 - 1)^{-2}(x^6 - 1)(x^4 - 1)^2(x^3 - 1)^{-1} \\ &\quad (x^2 - 1)^{-2} \\ P_{11}^{F+} &= (x^{34} - 1)(x^{17} - 1)^{-1}(x^{16} - 1)(x^{14} - 1)^4(x^{11} - 1)^4(x^4 - 1)^{-1}(x^2 - 1)^{-1} \\ P_{12}^{F+} &= (x^{38} - 1)(x^{32} - 1)^4(x^{19} - 1)^{-1}(x^{16} - 1)^{-4}(x^{13} - 1)^6(x^{10} - 1)^3(x^2 - 1)^2 \\ P_{13}^{F+} &= (x^{36} - 1)^5(x^{30} - 1)^8(x^{21} - 1)(x^{18} - 1)^{-5}(x^{15} - 1)^{-8}(x^{12} - 1)^6(x^{10} - 1)(x^9 - 1) \\ &\quad (x^8 - 1)(x^6 - 1)(x^5 - 1)^{-1}(x^4 - 1)^{-2}(x^3 - 1)^{-1}(x^2 - 1) \\ P_{14}^{F+} &= (x^{34} - 1)^{11}(x^{28} - 1)^{11}(x^{23} - 1)(x^{20} - 1)^5(x^{17} - 1)^{-11}(x^{14} - 1)^{-11}(x^{11} - 1)^3 \\ &\quad (x^4 - 1)^3(x^2 - 1)^{-3}(x - 1) \\ P_{15}^{F+} &= (x^{50} - 1)(x^{32} - 1)^{18}(x^{26} - 1)^8(x^{22} - 1)^6(x^{25} - 1)^{-1}(x^{19} - 1)^{14}(x^{16} - 1)^{-18} \\ &\quad (x^{13} - 1)^{-8}(x^{10} - 1)(x^8 - 1)(x^4 - 1)^{-1}(x^2 - 1)^{-2}(x - 1) \\ P_{16}^{F+} &= (x^{54} - 1)(x^{48} - 1)^6(x^{30} - 1)^{17}(x^{27} - 1)^{-1}(x^{24} - 1)^{-2}(x^{21} - 1)^{17}(x^{18} - 1)^{26} \\ &\quad (x^{15} - 1)^{-17}(x^{12} - 1)^{-4}(x^{10} - 1)^{-1}(x^7 - 1)(x^6 - 1)(x^5 - 1)(x^3 - 1)^{-1} \\ &\quad (x^2 - 1)^2(x - 1) \\ P_{17}^{F+} &= (x^{52} - 1)^7(x^{46} - 1)^{21}(x^{29} - 1)(x^{28} - 1)^{11}(x^{26} - 1)^{-7}(x^{23} - 1)^{-21}(x^{22} - 1) \\ &\quad (x^{20} - 1)^{38}(x^{17} - 1)^{31}(x^{14} - 1)^{-11}(x^{11} - 1)^{-1}(x^{10} - 1)^{-1}(x^8 - 1) \\ &\quad (x^4 - 1)^{-3}(x^2 - 1)(x - 1) \\ P_{18}^{F+} &= (x^{50} - 1)^{25}(x^{44} - 1)^{50}(x^{31} - 1)(x^{28} - 1)^7(x^{26} - 1)^4(x^{25} - 1)^{-25}(x^{22} - 1)^{-50} \\ &\quad (x^{19} - 1)^{52}(x^{16} - 1)^{26}(x^{13} - 1)^{-4}(x^8 - 1)^{-1}(x^4 - 1)^4(x^2 - 1)^{-3} \\ P_{19}^{F+} &= (x^{66} - 1)(x^{48} - 1)^{67}(x^{42} - 1)^{82}(x^{33} - 1)^{-1}(x^{30} - 1)^8(x^{27} - 1)^{29}(x^{24} - 1)^{-66} \\ &\quad (x^{21} - 1)^{-82}(x^{18} - 1)^{52}(x^{15} - 1)^{13}(x^{14} - 1)^{-1}(x^{12} - 1)^{-1}(x^9 - 1) \\ &\quad (x^8 - 1)(x^7 - 1)(x^6 - 1)^2(x^5 - 1)(x^4 - 1)^{-1}(x^3 - 1)^{-1}(x^2 - 1)^{-2} \\ P_{20}^{F+} &= (x^{70} - 1)(x^{64} - 1)^8(x^{46} - 1)^{122}(x^{40} - 1)^{97}(x^{35} - 1)^{-1}(x^{32} - 1)^{-8}(x^{29} - 1)^{34} \end{aligned}$$

$$\frac{(x^{26} - 1)^{85}(x^{23} - 1)^{-122}(x^{20} - 1)^{-97}(x^{17} - 1)^{35}(x^{14} - 1)^5(x^8 - 1)^{-1}}{(x^4 - 1)(x^2 - 1)^3} \quad (\text{A.8})$$

and from these we find that the degrees of the multiplicity of the eigenvalue +1 are 1, 0, 0, 1, 1, 2, 1, 2, 1, 4, 7, 11, 8, 10, 20, 47, 69, 86, 103, 162, ... (A.9)

where again there is a “mod 4” effect.

Appendix A.3. Characteristic polynomials $P_{L_h}^C$

The characteristic polynomials $P_{L_h}^C$ for $T_C(-1; L_h)$ have been well analyzed in [19] and are listed in appendix A of that paper to $L_h = 50$. The degree of the polynomials are the Lucas numbers which satisfy the recursion relation (A.1) with initial conditions $L(0) = 2$, $L(1) = 1$ and which have the generating function

$$G^C = \frac{1 + 2t}{(1 - t - t^2)} \quad (\text{A.10})$$

From the long list of [19] we find that the degrees of the multiplicity of the eigenvalue +1 are

$$1, 1, 2, 3, 0, 4, 1, 7, 8, 13, 2, 26, 9, 49, 38, 107, 28, 228, 49, 501, 324, 1101, 258, 2766, 469, 5845, 3790, 13555, 2376, 35624, 5813, 75807, 38036, 180213, 30482, 480782, 69593, 1047429, 485658, 2542453, 385020, 6794812, 914105, 15114481, 9570844, 36794329, 5212354, 101089306, 12602653, 222317557, \dots \quad (\text{A.11})$$

where we find a “mod 6” effect.

Appendix A.4. Characteristic polynomials $P_{L_h}^{C0+}$

The degrees of the polynomials $P_{L_h}^{C0+}$ are discussed in appendix B of [12] and are the series A129526 in the OEIS [45]. However, an explicit form is not known.

We have computed the characteristic polynomials in the less restrictive case of the momentum $P = 0$ sector. The degrees of the polynomials follow the series A000358 in the OEIS [45], which is given by the formula

$$\frac{1}{L_h} \sum_{n|L_h} \phi\left(\frac{L_h}{n}\right) [F(n-2) + F(n)] \quad (\text{A.12})$$

where $\phi(n)$ is Euler’s totient function (the number of positive integers $< n$ which are relatively prime with n). In particular when L_h is prime (A.12) specializes to

$$1 + \frac{F(L_h - 2) + F(L_h) - 1}{L_h} \quad (\text{A.13})$$

which grows as $N_G^{L_h}$.

The order of the restricted positive parity polynomial P^{C0+} is greater than the negative parity polynomial P^{C0-} and thus P^{C0+} also grows as $N_G^{L_h}$.

The first 29 polynomials are

$$\begin{aligned} P_1^{C0+} &= (x - 1) \\ P_2^{C0+} &= (x^4 - 1)(x^2 - 1)^{-1} \\ P_3^{C0+} &= (x^3 - 1)(x - 1)^{-1} \end{aligned}$$

$$\begin{aligned}
P_4^{C0+} &= (x^2 - 1)^2(x - 1)^{-1} \\
P_5^{C0+} &= (x^2 - 1)^2(x - 1)^{-1} \\
P_6^{C0+} &= (x^4 - 1)(x^3 - 1)(x^2 - 1)^{-1} \\
P_7^{C0+} &= (x^4 - 1)^2(x^2 - 1)^{-2}(x - 1) \\
P_8^{C0+} &= (x^{10} - 1)(x^5 - 1)^{-1}(x - 1)(x^2 - 1) \\
P_9^{C0+} &= (x^3 - 1)(x - 1)^2(x^2 - 1)^2 \\
P_{10}^{C0+} &= (x^8 - 1)(x^7 - 1)(x^2 - 1)^{-1}(x - 1) \\
P_{11}^{C0+} &= (x^5 - 1)^2(x^4 - 1)^3(x^2 - 1)^{-3} \\
P_{12}^{C0+} &= (x^{18} - 1)(x^9 - 1)^{-1}(x^6 - 1)(x^4 - 1)(x^3 - 1)^2(x^2 - 1)(x - 1)^{-1} \\
P_{13}^{C0+} &= (x^7 - 1)^3(x^2 - 1)^6(x - 1)^{-2} \\
P_{14}^{C0+} &= (x^{16} - 1)^3(x^{11} - 1)(x^8 - 1)^{-3}(x^5 - 1)(x^4 - 1)(x^2 - 1)^3(x - 1)^{-1} \\
P_{15}^{C0+} &= (x^9 - 1)^4(x^6 - 1)^2(x^4 - 1)^4(x^3 - 1)^3(x^2 - 1)^{-4}(x - 1)^{-1} \\
P_{16}^{C0+} &= (x^{26} - 1)(x^{14} - 1)^3(x^{13} - 1)^{-1}(x^{10} - 1)^3(x^7 - 1)^{-2}(x^5 - 1)^3(x^4 - 1)^5 \\
&\quad (x^2 - 1)^{-4}(x - 1) \\
P_{17}^{C0+} &= (x^{11} - 1)^6(x^8 - 1)^8(x^4 - 1)^{-2}(x^2 - 1)^4(x - 1)^3 \\
P_{18}^{C0+} &= (x^{24} - 1)^6(x^{18} - 1)^3(x^{15} - 1)(x^{12} - 1)^{-5}(x^9 - 1)^3(x^6 - 1)^{-1}(x^4 - 1) \\
&\quad (x^3 - 1)^4(x^2 - 1)^8(x - 1)^3 \\
P_{19}^{C0+} &= (x^{13} - 1)^8(x^{10} - 1)^{18}(x^7 - 1)^3(x^5 - 1)^{-6}(x^4 - 1)^5(x^2 - 1)^{-3}(x - 1)^2 \\
P_{20}^{C0+} &= (x^{34} - 1)(x^{22} - 1)^{15}(x^{17} - 1)^{-1}(x^{16} - 1)^2(x^{14} - 1)^6(x^{11} - 1)^{-8}(x^8 - 1) \\
&\quad (x^7 - 1)^4(x^4 - 1)^{17}(x^2 - 1)^{-12} \\
P_{21}^{C0+} &= (x^{15} - 1)^{10}(x^{12} - 1)^{27}(x^9 - 1)^{12}(x^6 - 1)^3(x^5 - 1)(x^4 - 1)^9(x^3 - 1)^7 \\
&\quad (x^2 - 1)^{-1}(x - 1)^{-3} \\
P_{22}^{C0+} &= (x^{32} - 1)^{10}(x^{26} - 1)^{14}(x^{20} - 1)^{15}(x^{19} - 1)(x^{16} - 1)^{-10}(x^{13} - 1)^{14} \\
&\quad (x^{10} - 1)^{-9}(x^7 - 1)(x^5 - 1)^6(x^4 - 1)^2(x^2 - 1)^{22}(x - 1)^{-2} \\
P_{23}^{C0+} &= (x^{17} - 1)^{13}(x^{14} - 1)^{45}(x^{11} - 1)^{43}(x^8 - 1)^4(x^7 - 1)^{15}(x^4 - 1)^5 \\
&\quad (x^2 - 1)^{16}(x - 1)^{-3} \\
P_{24}^{C0+} &= (x^{42} - 1)(x^{30} - 1)^{45}(x^{24} - 1)^{27}(x^{21} - 1)^{-1}(x^{18} - 1)^{16}(x^{15} - 1)^{-20} \\
&\quad (x^{12} - 1)^9(x^{10} - 1)^{10}(x^9 - 1)^2(x^8 - 1)^3(x^6 - 1)^9(x^5 - 1)^{-10} \\
&\quad (x^4 - 1)^{27}(x^3 - 1)^{12}(x^2 - 1)^{-23} \\
P_{25}^{C0+} &= (x^{19} - 1)^{16}(x^{16} - 1)^{92}(x^{13} - 1)^{116}(x^{10} - 1)^{20}(x^8 - 1)^{-8}(x^5 - 1)^5 \\
&\quad (x^4 - 1)^{41}(x^2 - 1)^{-33}(x - 1)^2 \\
P_{26}^{C0+} &= (x^{40} - 1)^{15}(x^{34} - 1)^{42}(x^{28} - 1)^{105}(x^{23} - 1)(x^{22} - 1)^{20}(x^{20} - 1)^{-15} \\
&\quad (x^{17} - 1)^{36}(x^{16} - 1)(x^{14} - 1)^{-45}(x^{11} - 1)^9(x^8 - 1)^{-1} \\
&\quad (x^7 - 1)^{28}(x^4 - 1)^{16}(x^2 - 1)^{26}(x - 1)^4 \\
P_{27}^{C0+} &= (x^{21} - 1)^{19}(x^{18} - 1)^{155}(x^{15} - 1)^{263}(x^{12} - 1)^{92}(x^9 - 1)^{-27}(x^7 - 1) \\
&\quad (x^5 - 1)^{26}(x^4 - 1)^{17}(x^3 - 1)^{19}(x^6 - 1)^7(x - 1)^9(x^2 - 1)^{67} \\
P_{28}^{C0+} &= (x^{50} - 1)(x^{38} - 1)^{120}(x^{32} - 1)^{168}(x^{26} - 1)^{110}(x^{25} - 1)^{-1}(x^{22} - 1)^{15} \\
&\quad (x^{20} - 1)^5(x^{19} - 1)^{-54}(x^{16} - 1)^{42}(x^{13} - 1)^{-26}(x^{11} - 1)^6 \\
&\quad (x^{10} - 1)(x^8 - 1)^{43}(x^5 - 1)^4(x^4 - 1)^{55}(x^2 - 1)^{-10}(x - 1)^2
\end{aligned}$$

$$P_{29}^{C0+} = (x^{23} - 1)^{23}(x^{20} - 1)^{205}(x^{17} - 1)^{581}(x^{14} - 1)^{364}(x^{11} - 1)^{36}(x^7 - 1)^{-14} \\ (x^{10} - 1)^{15}(x^5 - 1)^{-5}(x^4 - 1)^{131}(x^2 - 1)^{-115} \quad (\text{A.14})$$

and from these we find that the degrees of the multiplicity of the eigenvalue +1 are

$$1, 2, 2, 3, 3, 5, 5, 8, 9, 14, 16, 26, 31, 49, 64, 99, 133, 209, 291, 455, 657, 1022, 1510, 2359, \\ 3545, 5536, 8442, 13201, 20319, 31836, 49353, 77436, 120711, 189674, 296854, 467160, \\ 733363, 1155647, 1818594, 2869378, 4524081, 7146483, \dots \quad (\text{A.15})$$

where we find there is a “mod 6” effect.

Appendix B. Partition functions at $z = -1$

Successive powers of transfer matrices always satisfy a linear recursion relation, since any matrix satisfies its own characteristic polynomial. Therefore, any linear function of the matrix or its components which is independent of the power of the matrix will also satisfy the same linear recursion relation. The usual functions involved in creating partition functions from transfer matrices, the trace of the matrix, dot products with boundary vectors, and modified traces to account for Möbius and Klein bottle boundary conditions, all cause the respective partition functions to satisfy the same linear recursion relation as their transfer matrix, its characteristic polynomial. In particular, the Klein bottle partition function $Z_{L_v, L_h}^{KC}(z)$ satisfies the same linear recursion relation in L_v as the torus $Z_{L_v, L_h}^{CC}(z)$, since it is constructed from the same transfer matrix $T_C(z; L_h)$, and the cylinder partition function $Z_{L_v, L_h}^{CF}(z)$ satisfies the same recursion relation in L_v as the Möbius partition function $Z_{L_v, L_h}^{MF}(z)$ since they are both constructed from the same transfer matrix $T_F(z; L_h)$.

Therefore, the generating functions for the partition functions for a given L_h and for general z are rational functions in z and $x = L_v$ whose denominators are the characteristic polynomials of the L_h transfer matrix and whose numerators are polynomials given by the product of the characteristic polynomial and the initial terms of the series (the numerator has degree 1 less in x than the degree of the characteristic polynomial).

When the transfer matrix can be block diagonalized and the boundary vector dot products cause the partition function to be a function of only a restricted set of matrices in the direct sum, the partition function will satisfy a recursion relation of smaller order than the order of the full transfer matrix. As an example, $T_C(z; L_h)$ can be block diagonalized into different momentum sectors, and $Z_{L_v, L_h}^{FC}(z)$ is only a function of the reflection symmetric zero momentum sector 0^+ , so that the cylinder $Z_{L_v, L_h}^{FC}(z)$ will satisfy a recursion relation in L_v of the order of the 0^+ sector and not the order of the full $T_C(z; L_h)$ matrix. Likewise, $Z_{L_v, L_h}^{FF}(z)$ satisfies a recursion relation in L_v of the order of the positive parity sector of $T_F(z; L_h)$.

Beyond restrictions to particular matrix sectors, however, in general the polynomials in the numerator and denominator of the generating functions do not partially cancel, regardless of the initial conditions of the recursion relation, so that partition functions in z generally satisfy a recursion relation of the same order as its transfer matrix. This holds generically for hard hexagons and hard squares even if at particular values of z some cancellations can occur in the generating function.

For hard squares at $z = -1$ the denominators of the generating functions simplify to the expressions given in appendix A, whose orders grow according to the order of

the transfer matrices. The numerators, however, are such that massive cancellations occur, so that the partition functions as a function of $x = L_v$ at $z = -1$ satisfy linear recursion relations of much smaller degree than the partition function does for general z . The form of the numerator is dependent on the initial conditions of the recursion relation, that is, the partition function value at $z = -1$ for the first several values of L_v . This, in turn, is dependent on boundary conditions: both the torus and the Klein bottle partition functions satisfy the same linear recursion relation of their transfer matrix $T_C(-1; L_h)$, but the numerators of their generating functions are different, so that the Klein bottle exhibits much more massive cancellations than the torus for a given L_h . Likewise, the cylinder $Z_{L_v, L_h}^{CF}(-1)$ and the Möbius band have different recursion relation orders due to different amounts of cancellations at $z = -1$.

The cylinder has the property that for odd L_h , $Z_{L_v, L_h}^{FC}(-1) = -2$ whenever $\gcd(L_h - 1, L_v) = 0 \pmod{3}$, and $Z_{L_v, L_h}^{FC}(-1) = 1$ otherwise [21]. Therefore, the linear recursion relation of $Z_{L_v, L_h}^{FC}(-1)$ for odd L_h is always of order 1 or 2, even though for generic z the partition function $Z_{L_v, L_h}^{FC}(z)$ satisfies a linear recursion relation of the order of the 0^+ sector of the $T_C(z; L_h)$ transfer matrices, which grows as $N_G^{L_h}$. The initial conditions for the cylinder for odd L_h , therefore, are able to effect incredible cancellations to its generating function whose denominators are given in Appendix A.

In [19] it was proven that for the torus partition function, $Z_{L_v, L_h}^{CC}(-1) = 1$ whenever L_v, L_h are co-prime. Since for each L_h the torus at $z = -1$ satisfies a linear recursion relation, its initial conditions happen to be exactly suited to allow for this number theoretic property. This property does not extend to other boundary conditions even when they satisfy the same overall linear recursion relation. The Klein bottle satisfies the same $T_C(-1; L_h)$ linear recursion relation that the torus also satisfies, but its initial conditions do not cause it to share in the torus' co-primality property.

A repeating sequence with period n will have a generating function of the form $p(x)/(1 - x^n)$. Therefore, since all of the eigenvalues of the transfer matrices $T_C(-1; L_h)$ and $T_F(-1; L_h)$ are roots of unity, as long as the denominators have only square-free factors, the sequences of partition function values at $z = -1$ will be repeating, with a period given by the lcm of the exponents n_j in the factors $(1 - x^{n_j})$. Most sequences below are repeating, with a period often much larger than the order of the transfer matrix. For the limited cases considered below, all generating functions along a periodic direction (including a twist for Möbius bands and Klein bottles) are repeating. Along the free direction, the sequences are not always repeating; the cylinder for $L_h = 0 \pmod{4}$ is non-repeating and the free-free partition function is non-repeating for four of the L_h considered. In [22] a general form for the generating functions of $Z_{L_v, L_h}^{FC}(-1)$ for even L_h is conjectured, along with the conjecture that for even L_h the only repeating sequences for $Z_{L_v, L_h}^{FC}(-1)$ are when $L_h = 2 \pmod{4}$. We make the following conjecture:

Conjecture 1 *Along a periodic direction (including twists) all generating functions are repeating.*

We further find below that along the periodic direction, all repeating sequences are sums of repeating sub-sequences of period p_j which have value zero except at locations $p_j - 1 \pmod{p_j}$ where their value is an integer multiple of p_j . Often the value is exactly p_j . Therefore, the generating functions along a periodic direction are logarithmic derivatives of a product of factors of the form $(1 - x^{p_j})^{m_j}$, where m_j is an integer. We conjecture that this always holds:

Conjecture 2 *Along a periodic direction (including twists), all generating functions are logarithmic derivatives of products of the form $\prod_j (1 - x^{p_j})^{m_j}$, where p_j and m_j are integers.*

As it turns out, for the limited cases considered below, we find surprisingly that the generating functions for the torus and the cylinder along the periodic direction are exactly the negative of the logarithmic derivative of the characteristic polynomial of their transfer matrices at $z = -1$, so that we have the further conjecture:

Conjecture 3 *The generating functions of the torus and cylinder (along the periodic direction) are equal to the negative of the logarithm of their characteristic polynomials, that is, $G_{L_h}^{CC} = -\frac{d}{dx} \ln(P_{L_h}^{CC})$ and $G_{L_h}^{CF} = -\frac{d}{dx} \ln(P_{L_h}^{CF})$, respectively.*

This is similar to a conjecture in [46]. We note that this does not hold for general z , nor for Möbius bands or Klein bottles at $z = -1$. Due to this conjecture, we can use the results from appendix Appendix A to further the tables of periods for the sequences $Z_{L_v, L_h}^{CC}(-1)$ and $Z_{L_v, L_h}^{CF}(-1)$, where we notice a mod 3 pattern.

For $Z_{L_v, L_h}^{CC}(-1)$, for $L_h = 0 \pmod 3$ we conjecture that the periods are given by the $\text{lcm}(L_h, 2L_h, \dots, nL_h)$, where n is often given by $n = L_h/3 - 1$.

For $Z_{L_v, L_h}^{CF}(-1)$, for $L_h = 1 \pmod 3$ we conjecture that the periods are given by the $\text{lcm}(6, 12, \dots, 6n)$, where n is often $2(L_h - 4)/3 + 1$.

We also note that the periods of the cylinder (along the periodic L_v direction), the Möbius band, and the free-free plane are all equal, and the periods of the Klein bottle and cylinder (along the free L_v direction) are equal.

Below we list both the generating functions and tables of values for all boundary conditions, since number theoretic properties such as the torus's co-primality property can be missed by simply considering the generating functions. The periods of repeating sequences are tabulated, along with the minimal order of the recursion relations. All generating functions listed were determined by computing all partition function values up to the order of the transfer matrix and canceling the numerator and denominators of the generating function to arrive at the minimal order linear recursion relation; however, we extend the table of values to higher L_h .

Appendix B.1. The torus $Z_{L_v, L_h}^{CC}(-1)$

$L_h \setminus L_v$	1	2	3	4	5	6	7	8	9	10	11	12	13	14	15	16	17	18	19	20
1	1	1	1	1	1	1	1	1	1	1	1	1	1	1	1	1	1	1	1	1
2	1	-1	1	3	1	-1	1	3	1	-1	1	3	1	-1	1	3	1	-1	1	3
3	1	1	4	1	1	4	1	1	4	1	1	4	1	1	4	1	1	4	1	1
4	1	3	1	7	1	3	1	7	1	3	1	7	1	3	1	7	1	3	1	7
5	1	1	1	1	-9	1	1	1	1	11	1	1	1	1	-9	1	1	1	1	11
6	1	-1	4	3	1	14	1	3	4	-1	1	18	1	-1	4	3	1	14	1	3
7	1	1	1	1	1	1	1	1	1	1	1	1	1	-27	1	1	1	1	1	1
8	1	3	1	7	1	3	1	7	1	43	1	7	1	3	1	7	1	3	1	47
9	1	1	4	1	1	4	1	1	40	1	1	4	1	1	4	1	1	76	1	1
10	1	-1	1	3	11	-1	1	43	1	9	1	3	1	69	11	43	1	-1	1	13
11	1	1	1	1	1	1	1	1	1	1	1	1	1	1	1	1	1	1	1	1
12	1	3	4	7	1	18	1	7	4	3	1	166	1	3	4	7	1	126	1	7
13	1	1	1	1	1	1	1	1	1	1	1	1	-51	1	1	1	1	1	1	1
14	1	-1	1	3	1	-1	-27	3	1	69	1	3	1	55	1	451	1	-1	1	73
15	1	1	4	1	-9	4	1	1	4	11	1	4	1	1	174	1	1	4	1	11

Table B1. $Z_{L_v, L_h}^{CC}(-1)$

The generating functions $G_{L_h}^{CC}$ as a function of $x = L_v$ are given below.

$$\begin{aligned}
G_1^{CC} &= \frac{1}{(1-x)}, & G_2^{CC} &= G_1^{CC} + \frac{4x^3}{(1-x^4)} - \frac{2x}{(1-x^2)}, & G_3^{CC} &= G_1^{CC} + \frac{3x^2}{(1-x^3)}, \\
G_4^{CC} &= G_2^{CC} + \frac{4x}{(1-x^2)}, & G_5^{CC} &= G_1^{CC} + \frac{20x^9}{(1-x^{10})} - \frac{10x^4}{(1-x^5)}, \\
G_6^{CC} &= G_3^{CC} - G_1^{CC} + G_2^{CC} + \frac{12x^5}{(1-x^6)}, & G_7^{CC} &= G_1^{CC} + \frac{56x^{27}}{(1-x^{28})} - \frac{28x^{13}}{(1-x^{14})}, \\
G_8^{CC} &= G_4^{CC} + \frac{40x^9}{(1-x^{10})}, & G_9^{CC} &= G_3^{CC} + \frac{36x^{17}}{(1-x^{18})} + \frac{36x^8}{(1-x^9)}, \\
G_{10}^{CC} &= G_2^{CC} + \frac{70x^{13}}{(1-x^{14})} + \frac{10x^4}{(1-x^5)} + \frac{40x^7}{(1-x^8)}, \\
G_{11}^{CC} &= G_1^{CC} + \frac{110x^{54}}{(1-x^{55})} + \frac{176x^{43}}{(1-x^{44})} - \frac{88x^{21}}{(1-x^{22})}.
\end{aligned} \tag{B.1}$$

$Z^{CC} L_h$	1	2	3	4	5	6	7	8	9	10	11
T_C order	2	3	4	7	11	18	29	47	76	123	199
min rec order	1	3	3	4	6	8	15	12	18	24	77
period	1	4	3	4	10	12	28	20	18	280	220

Table B2. The minimal order of the recursion relation and the period of the repeating sequence of $Z_{L_v, L_h}^{CC}(-1)$ as a function of L_v .

Appendix B.2. The Klein bottle $Z_{L_v, L_h}^{KC}(-1)$ with twist in L_v direction

$L_h \setminus L_v$	1	2	3	4	5	6	7	8	9	10	11	12	13	14	15	16	17	18	19	20
1	1	1	1	1	1	1	1	1	1	1	1	1	1	1	1	1	1	1	1	1
2	-1	-3	-1	1	-1	-3	-1	1	-1	-3	-1	1	-1	-3	-1	1	-1	-3	-1	1
3	-1	-1	2	-1	-1	2	-1	-1	2	-1	-1	2	-1	-1	2	-1	-1	2	-1	-1
4	-1	5	-1	1	-1	5	-1	1	-1	5	-1	1	-1	5	-1	1	-1	5	-1	1
5	-1	3	-1	3	-1	3	-1	3	-1	3	-1	3	-1	3	-1	3	-1	3	-1	3
6	1	-5	4	-1	1	-2	1	-1	4	-5	1	2	1	-5	4	-1	1	-2	1	-1
7	1	-3	1	5	1	-3	1	5	1	-3	1	5	1	-3	1	5	1	-3	1	5
8	1	7	1	3	1	7	1	3	1	7	1	3	1	7	1	3	1	7	1	3
9	1	5	4	5	1	8	1	5	4	5	1	8	1	5	4	5	1	8	1	5
10	-1	-7	-1	-3	-1	-7	13	5	-1	-7	-1	-3	-1	-7	-1	5	-1	-7	-1	-3
11	-1	-5	-1	3	9	-5	-1	3	-1	5	-1	3	-1	-5	9	3	-1	-5	-1	13
12	-1	9	2	5	-1	12	-1	5	2	9	-1	8	-1	9	2	5	-1	12	-1	5
13	-1	7	-1	7	-1	7	13	7	-1	7	-1	7	-1	21	-1	7	-1	7	-1	7
14	1	-9	1	3	1	-9	1	-29	1	1	23	3	1	-9	1	3	1	-9	1	13

Table B3. $Z_{L_v, L_h}^{KC}(-1)$

The generating functions $G_{L_h}^{KC}$ as a function of $x = L_v$ are given below.

$$\begin{aligned}
G_1^{KC} &= \frac{1}{(1-x)}, & G_2^{KC} &= -G_1^{KC} + \frac{4x^3}{(1-x^4)} - \frac{2x}{(1-x^2)}, & G_3^{KC} &= -G_1^{KC} + \frac{3x^2}{(1-x^3)}, \\
G_4^{KC} &= -G_2^{KC} - 2G_1^{KC} + \frac{4x}{(1-x^2)}, & G_5^{KC} &= G_4^{KC} + G_2^{KC} + G_1^{KC}, \\
G_6^{KC} &= -G_4^{KC} + G_3^{KC} + G_1^{KC}, & G_7^{KC} &= 2G_2^{KC} + 3G_1^{KC}, & G_8^{KC} &= G_4^{KC} + 2G_1^{KC},
\end{aligned}$$

$$G_9^{KC} = G_5^{KC} + G_3^{KC} + 3G_1^{KC}, \quad G_{10}^{KC} = -G_8^{KC} - \frac{14x^{13}}{(1-x^{14})} + \frac{8x^7}{(1-x^8)} + \frac{14x^6}{(1-x^7)},$$

$$G_{11}^{KC} = G_7^{KC} - 2G_1^{KC} + \frac{10x^4}{(1-x^5)}. \quad (\text{B.2})$$

$Z^{KC} L_h$	1	2	3	4	5	6	7	8	9	10	11
T_C order	2	3	4	7	11	18	29	47	76	123	199
min rec order	1	3	2	4	2	5	3	4	4	20	7
period	1	4	3	4	2	12	4	4	6	56	20

Table B4. The minimal order of the recursion relation and the period of the repeating sequence of $Z_{L_v, L_h}^{KC}(-1)$ as a function of L_v .

Appendix B.3. The cylinder $Z_{L_v, L_h}^{FC}(-1) = Z_{L_h, L_v}^{CF}(-1)$

$L_h \setminus L_v$	1	2	3	4	5	6	7	8	9	10	11	12	13	14	15	16	17	18	19	20
1	1	1	1	1	1	1	1	1	1	1	1	1	1	1	1	1	1	1	1	1
2	-1	-1	1	1	-1	-1	1	1	-1	-1	1	1	-1	-1	1	1	-1	-1	1	1
3	-2	1	1	-2	1	1	-2	1	1	-2	1	1	-2	1	1	-2	1	1	-2	1
4	-1	3	-3	5	-5	7	-7	9	-9	11	-11	13	-13	15	-15	17	-17	19	-19	21
5	1	1	1	1	1	1	1	1	1	1	1	1	1	1	1	1	1	1	1	1
6	2	-1	1	4	-1	-1	4	1	-1	2	1	1	2	-1	1	4	-1	-1	4	1
7	1	1	1	1	1	1	1	1	1	1	1	1	1	1	1	1	1	1	1	1
8	-1	3	5	5	3	7	1	1	-1	3	-3	5	3	7	1	9	-1	3	-3	5
9	-2	1	1	-2	1	1	-2	1	1	-2	1	1	-2	1	1	-2	1	1	-2	1
10	-1	-1	1	1	9	-1	1	1	-11	-1	1	11	9	-1	1	-9	-11	-1	11	11
11	1	1	1	1	1	1	1	1	1	1	1	1	1	1	1	1	1	1	1	1
12	2	3	-3	8	-5	7	8	9	-9	14	-11	13	2	15	-15	8	-17	19	-4	21
13	1	1	1	1	1	1	1	1	1	1	1	1	1	1	1	1	1	1	1	1
14	-1	-1	1	1	-1	13	1	1	13	-1	15	1	-1	-15	1	15	-15	-1	-13	15
15	-2	1	1	-2	1	1	-2	1	1	-2	1	1	-2	1	1	-2	1	1	-2	1
16	-1	3	5	5	3	7	1	33	-1	3	13	5	3	7	-31	9	-1	35	-3	5

Table B5. $Z_{L_v, L_h}^{FC}(-1) = Z_{L_h, L_v}^{CF}(-1)$

The generating functions $G_{L_h}^{FC}$ as a function of $x = L_v$ are given below. For odd L_h there are only two cases:

$$G_{3n\pm 1}^{FC} = \frac{1}{(1-x)} \quad G_{3n}^{FC} = G_{3n\pm 1}^{FC} - \frac{3}{(1-x^3)}$$

For even L_h :

$$G_2^{FC} = G_1^{FC} - \frac{2(1+x)}{(1-x^4)}, \quad G_4^{FC} = \frac{x}{(1-x^2)} - \frac{(1-x)^2}{(1-x^2)^2}, \quad G_6^{FC} = -G_3^{FC} + G_2^{FC} + G_1^{FC},$$

$$G_8^{FC} = \frac{1}{5}G_4^{FC} - \frac{4(1+x)(1-x^5)^2}{5(1-x^{10})(1-x)^2} + \frac{8x(1+x)(x^3+3)(1-x^5)}{5(1-x^{10})(1-x)},$$

$$G_{10}^{FC} = G_2^{FC} + \frac{10x(1+x)(1+x^2)}{(1-x^8)} - \frac{10x(x^2+x+1)}{(1-x^7)},$$

$$G_{12}^{FC} = \frac{7}{9}G_4^{FC} - \frac{4(1-x^6)(1-x^9)}{(1-x^{18})} + \frac{2(1+x)(1-x^2)(1-x^3)^2}{3(1-x^6)^2} + \frac{(2x^5+2x^4+55x^3+55)}{9(1-x^6)},$$

$$G_{14}^{FC} = G_2^{FC} + \frac{28x^3 p_{14}^{FC}}{(1-x^{16})} - \frac{14x^3(x^7+x^6+x^2+x+1)}{(1-x^{11})} - \frac{14x^3(1+x)}{(1-x^5)},$$

$$G_{16}^{FC} = \frac{243G_4^{FC} + 2108G_1^{FC}}{455} + \frac{16(1+x)(1-x^{13})p_{16;1}^{FC}}{13(1-x^{26})} + \frac{32(1+x)(1-x^7)p_{16;2}^{FC}}{7(1-x^{14})} + \frac{8(1-x^2)p_{16;3}^{FC}}{5(1-x^{10})}, \quad (\text{B.3})$$

$$\begin{aligned} p_{14}^{FC} &= x^{12} + x^{11} + x^7 + x^6 + x^5 + x^2 + x + 1, \\ p_{16;1}^{FC} &= -2x^{11} + 6x^9 - 3x^8 + 4x^7 - 9x^6 + 5x^5 - 5x^4 + 9x^3 - 4x^2 + 3x - 6, \\ p_{16;2}^{FC} &= -x^5 + 3x^3 - x^2 + x - 3, \\ p_{16;3}^{FC} &= 7x^7 + 7x^6 - 3x^5 + x^4 - 5x^3 + 12x^2 + 6x + 10. \end{aligned} \quad (\text{B.4})$$

$Z^{FC} L_h$	2	4	6	8	10	12	14	16
T_{C0+} order	2	3	5	8	14	26	49	99
min rec order	2	3	5	7	13	15	25	29
period	4	-	12	-	56	-	880	-

Table B6. The minimal order of the recursion relation and the period of the repeating sequence of $Z_{L_v, L_h}^{FC}(-1)$ as a function of L_v .

The generating functions $G_{L_h}^{CF}$ as a function of $x = L_v$ are given below.

$$\begin{aligned} G_1^{CF} &= \frac{6x^5}{(1-x^6)} - \frac{3x^2}{(1-x^3)} - \frac{2x}{(1-x^2)} + \frac{1}{(1-x)}, & G_2^{CF} &= \frac{4x^3}{(1-x^4)} - \frac{2x}{(1-x^2)} + \frac{1}{(1-x)}, \\ G_3^{CF} &= \frac{8x^7}{(1-x^8)} - \frac{4x^3}{(1-x^4)} + \frac{1}{(1-x)}, & G_4^{CF} &= G_1^{CF} + G_2^{CF} + \frac{4x}{(1-x^2)} - \frac{1}{(1-x)}, \\ G_5^{CF} &= G_3^{CF} + \frac{10x^9}{(1-x^{10})} - \frac{2x}{(1-x^2)}, & G_6^{CF} &= 2G_2^{CF} + \frac{14x^{13}}{(1-x^{14})} + \frac{2x}{(1-x^2)} - \frac{1}{(1-x)}, \\ G_7^{CF} &= G_3^{CF} - G_2^{CF} + G_1^{CF} + \frac{18x^{17}}{(1-x^{18})} + \frac{12x^{11}}{(1-x^{12})}, \\ G_8^{CF} &= -G_3^{CF} + \frac{22x^{21}}{(1-x^{22})} + \frac{32x^{15}}{(1-x^{16})} + \frac{4x^3}{(1-x^4)} + \frac{2}{(1-x)}, \\ G_9^{CF} &= G_6^{CF} - G_5^{CF} + G_2^{CF} + \frac{26x^{25}}{(1-x^{26})} + \frac{60x^{19}}{(1-x^{20})} + \frac{16x^7}{(1-x^8)} - \frac{24x^3}{(1-x^4)}, \\ G_{10}^{CF} &= G_4^{CF} - G_3^{CF} + G_2^{CF} + \frac{30x^{29}}{(1-x^{30})} + \frac{72x^{23}}{(1-x^{24})} + \frac{36x^{17}}{(1-x^{18})}. \end{aligned} \quad (\text{B.5})$$

$Z^{CF} L_h$	1	2	3	4	5	6	7	8	9	10
T_F order	2	3	5	8	13	21	34	55	89	144
min rec order	2	3	5	6	13	16	26	36	60	60
period	6	4	8	12	40	28	72	176	3640	360

Table B7. The minimal order of the recursion relation and the period of the repeating sequence of $Z_{L_v, L_h}^{CF}(-1)$ as a function of L_v .

$L_h \setminus L_v$	1	2	3	4	5	6	7	8	9	10	11	12	13	14	15	16	17	18	19	20
1	1	-1	-2	-1	1	2	1	-1	-2	-1	1	2	1	-1	-2	-1	1	2	1	-1
2	-1	-3	-1	1	-1	-3	-1	1	-1	-3	-1	1	-1	-3	-1	1	-1	-3	-1	1
3	-1	-1	-1	-5	-1	-1	-1	3	-1	-1	-1	-5	-1	-1	-1	3	-1	-1	-1	-5
4	-1	3	-4	-1	-1	6	-1	-1	-4	3	-1	2	-1	3	-4	-1	-1	6	-1	-1
5	-1	1	-1	-3	9	1	-1	5	-1	1	-1	-3	-1	1	9	5	-1	1	-1	-3
6	1	-5	1	3	1	-5	15	3	1	-5	1	3	1	-5	1	3	1	-5	1	3
7	1	-3	-2	-3	1	12	1	5	-20	-3	1	0	1	-3	-2	5	1	12	1	-3
8	1	5	1	-3	1	5	1	-27	1	5	-21	-3	1	5	1	5	1	5	1	-3
9	1	3	1	-5	1	3	-13	3	1	-47	1	-5	27	3	1	3	1	3	1	5
10	-1	-7	-4	-3	-1	-4	-1	5	-40	-7	-1	72	-1	-7	26	5	-1	-4	-1	-3
11	-1	-5	-1	-1	-1	-5	-1	-9	-1	-5	87	-1	-1	93	-1	7	-35	-5	-1	-1
12	-1	7	-1	-5	-1	7	-1	3	-1	57	-1	-5	155	7	-1	-125	-1	7	-39	5

Table B8. $Z_{L_v, L_h}^{MF}(-1)$

Appendix B.4. The Möbius band $Z_{L_v, L_h}^{MF}(-1)$ with twist in the L_v direction

The generating functions $G_{L_h}^{MF}$ as a function of $x = L_v$ are given below.

$$\begin{aligned}
G_1^{MF} &= \frac{6x^5}{(1-x^6)} - \frac{3x^2}{(1-x^3)} - \frac{2x}{(1-x^2)} + \frac{1}{(1-x)}, & G_2^{MF} &= \frac{4x^3}{(1-x^4)} - \frac{2x}{(1-x^2)} - \frac{1}{(1-x)}, \\
G_3^{MF} &= \frac{8x^7}{(1-x^8)} - \frac{4x^3}{(1-x^4)} - \frac{1}{(1-x)}, & G_4^{MF} &= -G_2^{MF} + G_1^{MF} + \frac{4x}{(1-x^2)} - \frac{3}{(1-x)}, \\
G_5^{MF} &= G_3^{MF} - \frac{10x^9}{(1-x^{10})} + \frac{10x^4}{(1-x^5)} + \frac{2x}{(1-x^2)}, \\
G_6^{MF} &= 2G_2^{MF} - \frac{14x^{13}}{(1-x^{14})} + \frac{14x^6}{(1-x^7)} - \frac{2x}{(1-x^2)} + \frac{3}{(1-x)}, \\
G_7^{MF} &= G_3^{MF} + G_2^{MF} + G_1^{MF} + \frac{18x^{17}}{(1-x^{18})} - \frac{12x^{11}}{(1-x^{12})} - \frac{18x^8}{(1-x^9)} + \frac{12x^5}{(1-x^6)} + \frac{2}{(1-x)}, \\
G_8^{MF} &= -3G_3^{MF} - 5G_2^{MF} + \frac{22x^{21}}{(1-x^{22})} + \frac{32x^{15}}{(1-x^{16})} - \frac{22x^{10}}{(1-x^{11})} - \frac{6x}{(1-x^2)} - \frac{7}{(1-x)}, \\
G_9^{MF} &= -G_6^{MF} + G_3^{MF} + G_2^{MF} - \frac{26x^{25}}{(1-x^{26})} + \frac{60x^{19}}{(1-x^{20})} + \frac{26x^{12}}{(1-x^{13})} - \frac{50x^9}{(1-x^{10})} - \frac{2x}{(1-x^2)} + \frac{4}{(1-x)}, \\
G_{10}^{MF} &= 2G_7^{MF} - G_3^{MF} - G_1^{MF} - \frac{30x^{29}}{(1-x^{30})} - \frac{72x^{23}}{(1-x^{24})} + \frac{30x^{14}}{(1-x^{15})} + \frac{96x^{11}}{(1-x^{12})} - \frac{24x^5}{(1-x^6)} - \frac{3}{(1-x)}.
\end{aligned} \tag{B.6}$$

$Z_{L_h}^{MF}$	1	2	3	4	5	6	7	8	9	10
T_F order	2	3	5	8	13	21	34	55	89	144
min rec order	2	3	5	5	13	16	23	35	60	59
period	6	4	8	12	40	28	72	176	3640	360

Table B9. The minimal order of the recursion relation and the period of the repeating sequence of $Z_{L_v, L_h}^{MF}(-1)$ as a function of L_v .

$L_h \setminus L_v$	1	2	3	4	5	6	7	8	9	10	11	12	13	14	15	16	17	18	19	20
1	0	-1	-1	0	1	1	0	-1	-1	0	1	1	0	-1	-1	0	1	1	0	-1
2	-1	-1	1	1	-1	-1	1	1	-1	-1	1	1	-1	-1	1	1	-1	-1	1	1
3	-1	1	-1	-1	1	-1	1	1	-1	1	-1	-1	1	-1	1	1	-1	1	-1	-1
4	0	1	-1	2	-1	3	-2	3	-3	4	-3	5	-4	5	-5	6	-5	7	-6	7
5	1	-1	1	-1	1	1	-1	3	-1	1	-3	3	-1	1	3	-3	3	-1	3	-1
6	1	-1	-1	3	1	-3	1	5	-1	-5	3	5	-3	-3	5	3	-5	-1	5	1
7	0	1	1	-2	-1	1	2	3	-1	-2	-1	-1	4	3	-1	-2	-3	3	4	1
8	-1	1	1	3	3	5	3	3	3	3	-1	1	-3	-1	-3	1	-3	1	1	5
9	-1	-1	-1	-3	-1	-1	-1	3	3	1	5	1	5	5	1	1	-3	-5	-5	-5
10	0	-1	1	4	1	-5	-2	3	1	2	-1	3	-4	-7	7	10	-1	-7	-4	5
11	1	1	-1	-3	1	3	-1	-1	5	-1	1	1	-1	-3	-1	7	-1	-3	-3	3
12	1	1	-1	5	-3	5	-1	1	1	3	1	5	-1	17	-1	5	1	-1	-1	3
13	0	-1	1	-4	3	-3	4	-3	5	-4	-1	-1	2	1	-1	0	5	-3	10	-9

Table B10. $Z_{L_v, L_h}^{FF}(-1)$

Appendix B.5. The free-free plane $Z_{L_v, L_h}^{FF}(-1)$

The generating functions $G_{L_h}^{FF}$ as a function of $x = L_v$ are given below.

$$\begin{aligned}
G_1^{FF} &= \frac{2x^4(1+x)}{(1-x^6)} + \frac{1}{(1-x^3)} - \frac{1}{(1-x)}, & G_2^{FF} &= \frac{2x^2(1+x)}{(1-x^4)} - \frac{1}{(1-x)}, \\
G_3^{FF} &= \frac{2x^3(x-1)(1+x^2)}{(1-x^8)} + \frac{2x}{(1-x^2)} - \frac{1}{(1-x)}, \\
G_4^{FF} &= \frac{1}{3}G_1^{FF} - \frac{(1-x)^2}{3(1-x^2)^2} + \frac{x}{3(1-x^2)} + \frac{1}{3(1-x)}, \\
G_5^{FF} &= G_3^{FF} + \frac{10x^3(1-x) + 4(1-x)^2(2x^2+x+2)}{5(1-x^5)} + \frac{2}{5(1-x)}, \\
G_6^{FF} &= 2G_2^{FF} + \frac{2(1-x)(5x^5+10x^4+x^3-x^2+11x+9)}{7(1-x^7)} + \frac{3}{7(1-x)}, \\
G_7^{FF} &= G_3^{FF} + \frac{p_7^{FF}(x^6+x^3+1)(1-x^2)}{3(1-x^{18})} + \frac{(1-x)(1-x^2)^2(x^2+x+1)^2}{3(1-x^6)^2} + \frac{1}{3(1-x)}, \\
G_8^{FF} &= \frac{-3G_4^{FF} + G_1^{FF}}{11} + \frac{2(1+x)(1-x^{11})p_{8;1}^{FF}}{11(1-x^{22})} + \frac{2(1-x^8)p_{8;2}^{FF}}{(1-x^{16})} - \frac{15}{11(1-x)}, \\
G_9^{FF} &= G_3^{FF} + \frac{p_{9;1}^{FF}}{(1-x^{20})} + \frac{p_{9;2}^{FF}}{(1-x^{14})} + \frac{2(1-x)p_{9;3}^{FF}}{13(1-x^{13})} + \frac{2}{13(1-x)}, \\
G_{10}^{FF} &= \frac{1}{9}G_4^{FF} + \frac{4p_{10;1}^{FF}}{3(1-x^{18})} + \frac{2p_{10;2}^{FF}}{5(1-x^{15})} - \frac{p_{10;3}^{FF}}{2(1-x^{12})} - \frac{p_{10;4}^{FF}}{90(1-x^6)^2} + \frac{p_{10;5}^{FF}}{90(1-x^6)} + \frac{4}{15(1-x)}, \\
G_{11}^{FF} &= G_3^{FF} + \frac{p_{11;1}^{FF}}{(1-x^{34})} + \frac{p_{11;2}^{FF}}{(1-x^{16})} - \frac{2(1-x^2)p_{11;3}^{FF}}{7(1-x^{14})} + \frac{(1-x)p_{11;4}^{FF}}{11(1-x^{11})} + \frac{27}{77(1-x)}, \tag{B.7}
\end{aligned}$$

$$\begin{aligned}
p_7^{FF} &= x^9 + x^8 + 2x^6 - 7x^5 + 4x^4 - 4x^3 + 7x^2 - 2x + 1, \\
p_{8;1}^{FF} &= 8x^9 + 9x^7 - 2x^6 + x^5 + 5x^4 - 5x^3 - x^2 + 2x - 9, \\
p_{8;2}^{FF} &= -x^7 - x^6 - 2x^5 - x^4 + x + 2, \\
p_{9;1}^{FF} &= 2(2x^5 + x^4 - x - 2)(1+x^2)(1-x^{10}), \\
p_{9;2}^{FF} &= 2(-x^5 - x^3 + x^2 - x + 1)(1+x)(1-x^7), \\
p_{9;3}^{FF} &= 14x^{11} + 28x^{10} + 16x^9 + 17x^8 - 8x^7 - 7x^6 + 7x^5 + 21x^4 + 35x^3 + 36x^2 + 11x + 12,
\end{aligned}$$

$$\begin{aligned}
p_{10;1}^{FF} &= x(1-x)(x^6 + x^3 + 1)(1-x^6), \\
p_{10;2}^{FF} &= (1+x)(1-x^3)(2x^{10} - 4x^8 + 4x^7 + 4x^6 - 7x^5 + x^4 + 7x^3 - 4x^2 - 2x + 4), \\
p_{10;3}^{FF} &= (1-x^6)(5x^5 + 5x^4 - 4x^3 - 7x^2 + 7x + 4), \\
p_{10;4}^{FF} &= (1-x)(1-x^2)^2(37x^4 + 86x^3 + 111x^2 + 86x + 37), \\
p_{10;5}^{FF} &= (97x^3 + 97x^2 + 48x + 49)(1-x^2), \\
p_{11;1}^{FF} &= 2x^2(1+x)(1-x^{17})(x^{13} - 2x^9 + x^8 + x^6 + x^5 - x^4 - x^3 - x + 2), \\
p_{11;2}^{FF} &= (1-x^8)(x^7 + x^6 + x^5 - 3x^4 - x^3 + x^2 + 3x - 1), \\
p_{11;3}^{FF} &= 8x^{11} + 8x^{10} + 2x^9 + 9x^8 - 4x^7 - 4x^6 - 3x^5 + 11x^4 + 12x^3 + 12x^2 - x + 6, \\
p_{11;4}^{FF} &= -4x^9 - 8x^8 - 56x^7 - 16x^6 + 24x^5 + 20x^4 - 28x^3 - 32x^2 + 8x + 48. \tag{B.8}
\end{aligned}$$

$Z^{FF} L_h$	1	2	3	4	5	6	7	8	9	10	11
T_{F+} order	2	2	4	5	9	12	21	30	51	76	127
min rec order	2	2	4	5	9	9	17	21	31	35	51
period	6	4	8	-	40	28	-	-	3640	-	20944

Table B11. The minimal order of the recursion relation and the period of the repeating sequence of $Z_{L_v, L_h}^{FF}(-1)$ as a function of L_v .

Appendix C. Hard square equimodular curves as $|z| \rightarrow \infty$

Consider hard squares for a system of width $L_h = 2L$ sites. The boundary conditions can be free or periodic, but not restricted by parity or momentum. We wish to show that the transfer matrices $T_C(z; L_h)$ and $T_F(z; L_h)$ both have $2L$ branches of equimodular curves going out to $|z| \rightarrow \infty$.

Let A (resp. B) denote the maximally packed state with L particles occupying the even (resp. odd) numbered sites. Similarly, for $k \ll L$, let A_k denote the classes of states having $L - k$ particles of which $O(L)$ have positions overlapping with those of A and $O(1)$ overlap with those of B . More loosely, the states A_k have the same order as A , up to small local perturbations. The states B_k are similarly defined from B .

To discuss the $|z| \rightarrow \infty$ limit we replace z by z^{-1} and consider a perturbation theory for $|z| \ll 1$. After division by an overall factor, the Boltzmann weight of state A is 1, and each of the states in the class A_k have weight z^k .

To order zero (i.e., considering only states A and B) the transfer matrix is the permutation matrix of size 2, with eigenvalues $\lambda_1 = 1$ and $\lambda_2 = -1$.

To order $k \ll L$ it is easy to see that the only non-zero matrix elements connect an A -type state to a B -type state and vice versa. Physically this means that if we start from a state which has predominantly particles on the even sublattice, it will remain so forever: we stay in the same ordered phase. Mathematically it is not hard to see that this implies that the eigenvalues λ_1 and λ_2 will continue to just differ by an overall sign, order by order in perturbation theory. Other eigenvalues are $O(z)$, hence play no role since then cannot be equimodular with λ_1 and λ_2 .

The perturbative result $\lambda_1 + \lambda_2 = 0$ breaks down at an order k which is sufficiently high to create a domain wall across the strip/cylinder/torus between the two different ordered states. This happens precisely for $k = L$. It follows that $\lambda_1 + \lambda_2 = O(z^L)$,

implying that

$$\lambda_2/\lambda_1 = -1 + O(z^L). \quad (\text{C.1})$$

To obtain equimodularity, the left-hand side must be on the unit circle. For $|z| \ll 1$ this will happen when z^L is perpendicular to -1 , so that $\arg(z^L) = \pm\pi/2$. It follows that there are $2L$ equimodular curves going out of $z = 0$ with the angles

$$\arg(z) = \frac{(1 + 2k)\pi}{2L} \text{ with } k = 0, 1, \dots, 2L - 1. \quad (\text{C.2})$$

References

- [1] Onsager L 1944 Crystal statistics I: a two dimensional model with an order disorder transition Phys. Rev. 65, 117-149.
- [2] Nickel B 1999 On the singularity structure of the 2D Ising model susceptibility J. Phys. A 32, 3889-3906.
- [3] Nickel B 2000 On the singularity structure of the 2D Ising model susceptibility: addendum J. Phys. A 33, 1693-1711.
- [4] Orrick W P, Nickel B, Guttmann A J and Perk J H H 2001 The susceptibility of the square lattice Ising model: New developments J. Stat. Phys. 102, 795-841.
- [5] Chen Y, Guttmann A J, Nickel B and Perk J H H 2011 The Ising susceptibility scaling function J. Stat. Phys. 145, 549-590.
- [6] Baxter R J 1980 Hard hexagons: Exact Solution J. Phys. A 13 L61-L70.
- [7] Baxter R J 1982 Exactly Solved Models in Statistical Mechanics (New York: Academic Press).
- [8] Baxter R J and Pearce P A 1982, Hard hexagons: interfacial tension and correlation length J. Phys. A15, 897-910.
- [9] Gaunt D S and Fisher M E 1965 Hard-sphere lattice gasses. I. plane square lattice J. Chem. Phys. 43 2840.
- [10] Runnels L K and Combs L L 1965 Exact finite method of lattice statistics. I. Square and triangular lattice gases of hard molecules J. Chem. Phys. 45 2482.
- [11] Baxter R J, Enting I G and Tsang S K 1980 Hard-square lattice gas J. Stat. Phys. 22 465-489.
- [12] Ree F H and Chestnut D A 1966 Phase transition of a hard-core lattice gas. The square lattice with nearest-neighbor exclusion J. Chem. Phys. 45, 3983-4003.
- [13] Chan Y 2012 Series expansions from corner transformation renormalization group method: the hard-squares model J. Phys. A 45, 0850013.
- [14] Kamieniarsz G and Blöte H W J 1993 The non-interacting hard-square lattice gas: Ising universality J. Phys. A 26, 6679-6689.
- [15] Guo W and Blöte H W 2002 Finite size analysis of the hard square lattice gas Phys. Rev. E 66, 046140.
- [16] Guttmann A J 1987 Comment on ‘The exact location of partition function zeros; a new method for statistical mechanics’ J. Phys. A 20, 511-512.
- [17] Jensen I 2012, Comment on ‘Series expansions from corner transformation renormalization group method: the hard-squares model’ J.Phys. A 45,508001 (5pp).
- [18] Fendley P, Schoutens K and van Eerten H 2005 Hard squares with negative activity J. Phys. A 38 315-322.
- [19] Jonsson J 2006 Hard squares with negative activity and rhombus tilings of the plane Electron. J. Combin. 13 (1) #R67.
- [20] Jonsson J 2006 Hard squares with grids with diagonal boundary conditions <http://www.math.kth.se/~jakob/combin.html>
- [21] Jonsson J 2009 Hard squares with negative activity on cylinders with odd circumference Electron. J. Combin. 16, no 2 #R5.
- [22] Adamaszek M 2012 Hard squares on cylinders revisited arXiv:1202.1655.
- [23] Baxter R.J, 2011 Hard squares for $z = -1$ Ann. Comb. 15 185-195.
- [24] Assis M, Jacobsen J L, Jensen I, Maillard J-M and McCoy B M 2013 The hard hexagon partition function for complex fugacity J. Phys. A 46, 445202 (46pp).
- [25] Salas J and Sokal A.D 2001 Transfer matrices and partition-function zeros for antiferromagnetic Potts models. I. General theory and square lattice chromatic polynomial J. Stat. Phys. 104 609-699.
- [26] Jacobsen J L and Salas J 2001 Transfer matrices and partition-function zeros for antiferromagnetic Potts models. II. Extended results for square-lattice chromatic polynomial J. Stat. Phys. 104, 701-723.

- [27] Jacobsen J L, Salas J and Sokal A D 2003 Transfer matrices and partition-function zeros for antiferromagnetic Potts models. III. Triangular-lattice chromatic polynomial J. Stat. Phys. 112, 921-1017.
- [28] Jacobsen J Land Salas J 2006 Transfer matrices and partition-function zeros for antiferromagnetic Potts models. IV. Chromatic polynomial with cyclic boundary conditions J. Stat. Phys. 122, 705-760
- [29] Jacobsen J L and Salas J 2007 Phase diagram of the chromatic polynomial on a torus Nucl. Phys. B 783, 238-296 (2007)
- [30] Richard J-F and Jacobsen J L, 2006 Character decomposition of Potts model partition functions, I: Cyclic geometry Nucl. Phys. B 750, 250-264
- [31] Richard J-F and Jacobsen J L 2007 Eigenvalue amplitudes of the Potts model on a torus Nucl. Phys. B 769, 256-274.
- [32] Cherednik I V 1984 Factorizing particles on a half-line and root systems Teor. Mat. Fiz 61, 35.
- [33] Sklyanin E K 1988 Boundary conditions for integrable quantum systems J. Phys. A21, 2375.
- [34] Behrand R E and Pearce P A 1996 A construction of solutions to reflection equations for interaction-round-a-face models J. Phys. A29, 7827-7835.
- [35] Ahn C and You C-K 1998 Complete non-diagonal reflection matrices of RSOS/SOS and hard hexagon models J. Phys. A31, 2109-2121.
- [36] Joyce G S 1988 On the hard-hexagon model and the theory of modular functions Phil. Trans. R. Soc. Lond. A 326, 643-702.
- [37] Wood D W 1985, The exact location of partition function zeros; a new method for statistical mechanics J. Phys. A 18, L917-L921.
- [38] Wood D W 1987 The algebraic construction of partition function zeros: universality and algebraic cycles J. Phys. A 20, 3471-3493.
- [39] Baxter R J 1987 Chromatic polynomials of large triangular lattices J. Phys. A 20, 5241-5261.
- [40] Beraha S, Kahane J and Weiss N.J 1975 Limits of zeros of recursively defined polynomials Proc. Nat. Acad. Sci. USA 72 4209.
- [41] Beraha S, Kahane J and Weiss N.J 1978 in *Studies in Foundations and Combinatorics* (Advances in Mathematics Supplementary Studies, vol. 1) ed. G.-G. Rota (Academic Press, New York).
- [42] Beraha S, Kahane J and Weiss N.J 1980 Limits of chromatic zeros of some families of maps. J. Combin. Theory B 28 52-65.
- [43] Chang S-C, Jacobsen J L, Salas J and Shrock R 2004 Exact Potts model partition functions for strips of the triangular lattice J. Stat. Phys. 114, 763-823
- [44] Jacobsen J L 2007 Exact enumeration of Hamiltonian circuits, walks and chains in two and three dimensions J. Math. Phys 40 14667-78.
- [45] The On-Line Encyclopedia of Integer Sequences at <http://oeis.org>.
- [46] Abarenkova N, Angles d'Auriac J-Ch, Boukraa S, Hassani S, Maillard J-M, 1999 Rational dynamical zeta functions for birational transformations Physica A 264, 264-293.